Global Research journal of Natural Science and Technology (Grjnst)
Volume: 02 - Issue 3 (2024)
p.ISSN: 2790-7643 e.ISSN: 2790-7651
www.grjnst.com

The Porous Flow of Cu-Water and Cu-Kerosene Nano-fluids Between Two Parallel Squeezing Plates

Sadam Hussain

Department of physical and Numerical sciences,Qurtuba University of Science and information technology Peshawar KPK, Pakistan

Sadamhussain11201@gmail.com

Muhammad ziad

Department of Mathematics & statistics, Hazara University Mansehra KPK, Pakistan

muhammadziad004@gmail.com

Fasih ullah shah

Department of Mathematics & statistics, Hazara University Mansehra KPK, Pakistan

fasihshah744@gmail.com

Muhammad Safdar

Department of Mathematical Science's University of Lakki Marwawt,KPK, Pakistan

safdarbarki1245@gmail.com

Ubaid Ur Rehman

Department of Mathematics, Gomal University DI Khan KPK, Pakistan

ubrehmansh138@gmail.com

Abstract

Section one deals with introduction, aims and objectives and problem statement. Literature review and some basic preliminaries which are related to research work are described in chapter two. Section three addresses the two-dimensional (2D) boundary layer of magnetic flow of viscous fluid through a stretched wall/surface. Constant temperature is imposed at the stretched sheet. Suitable variables are utilized to acquire the nonlinear ordinary differential systems. Analytical solutions of governing system is obtained through HAM. Various graphs and tables are analyzed through sundry parameters. section four concentrates the steady magnetohydrodynamic (MHD) stagnation point

flow of viscous liquid through heat and mass transport. The fluid flow is generated by a permeable stretched wall and containing chemical species. The transformation technique utilizes similarity variables to simplify the nonlinear partial differential systems for flow field into ordinary differential systems. Convergent homotopic solutions are analyzed for the resulting nonlinear systems. Convergence interval is determined in view of numerical tables and graph. A detailed study of graphical features shows with various variables on velocity (fluid flow), temperature, concentration as well as the coefficient of skin-friction and the local Nusselt and Sherwood numbers are described in section five. Section six comprises with concluding remarks and future research work.

Keywords: Porous Flow, Cu-Water, Cu-Kerosene, Nano-fluids, Parallel Squeezing Plates

Introduction

1.1 Research summary

Section 1: The movement of fluid substances towards an elongated sheet has captured the interest of researchers, owing to its significant applications in various engineering developments such as polymer extrusion, the formation of plastic wires and films, paper manufacturing, glass fiber manufacture, food processing, crystal growth, and the analysis of liquid layers in condensation, among others. Crane [1] conducted research on the flow characteristics resulting from a stretched surface. In the existing body of literature, the majority of studies focus on the boundary layer flow through a stretched wall, assuming that the velocity of the stretched wall/plate is linearly related to the distance from a fixed origin. However, in reality, the stretched wall/sheet, especially in the context of plastic materials, may not exhibit a linear profile. There are broader technological applications for the investigation of flow and heat transfer characteristics through an exponentially stretched plate. For instance, in processes like strengthening and thinning of copper wires, the finishing product's quality is influenced by the rate of heat transport at the wall with exponential variations in stretching velocity. In such procedures, both the kinematics of stretching and concurrent heating or cooling play a crucial role in determining the end product's quality. A specific example in this context is observed in the plastic industry. Vajravelu and Cannon [2] discussed numerical solutions for a set of nonlinear third-order differential systems that emerge in the context of fluid flows through nonlinearly stretched wall/sheet. These solutions were derived through the application of a similarity transformation distinct from the one employed in addressing the linearly stretching sheet problem. Ariel [3] examined the steady, laminar flow arising from the stretching of a

sheet in three dimensions. The governing equations for this motion allow for a similarity solution. Through an analogy with the flow induced by a rotating disk, we show that the corresponding boundary value problem can be solved using a series of exponentially decaying functions. This solution proves to be highly efficient and accurate, eliminating the necessity of replacing numerical infinity in the integration range with a finite value. Andersson et al. [4] deliberated the movement of chemically reactive substances in the laminar flow through a flexible flat plate/wall. The viscous flow is propelled exclusively by the linear stretching of the plate, and the reactive species emanates from this plate/sheet. The substance experiences an isothermal and homogeneous one-stage reaction as it diffuses into the contiguous fluid materials.

Magnetic nanomaterials offer enhanced versatility as their physical features can be adjusted using an external magnetic field. Various devices, including pumps, MHD generators, boundary layer governor systems and bearings, are influenced by the interaction among electrically conductive materials and a magnetic pitch. The impact on the flow is heavily contingent on the location and strength of the useful magnetic pitch. The magnetic force that is applied modifies the scattered particles, affecting their concentration within the liquid and so influencing the flow's heat transmission characteristics. Magnetic nanofluids exhibit both fluid and magnetic aspects, finding exciting uses in optical agents, magneto-optical spectrum strainers, nonlinear optical substances, optical switches, and optical grids. Connecting materials and sink-float separation procedures both relies heavily on magnetic materials for the manufacturing of loudspeakers. Magneto nanomaterials are employed to guide particles along the arteries to tumors using electromagnets radiations, owing to the increased adhesiveness of magnetic nanoparticles to tumor cells compared to non-malignant cells. In human-safe electrically generated magnetic fields, these particles acquire more power than microparticles, especially in cancer treatment. Diverse applications of magnetic nanomaterials including drug delivery, hyperthermia, improving disparity in magnetic resonance imaging (MRI), and magnetized cell separation. Fadzilah [5] investigated the influences of the developing magnetic field while analyzing the steady MHD (magnetohydrodynamic) boundary layer fluid flow of a viscous (Newtonian material) and electrically conducting material through a stretched plate. Shakhaoath et al. [6] analyzed a numerical investigation have been conducted on unsteady laminar boundary-layer flows of a nanomaterial over a stretched wall using radiative aspects, considering the influence of a magnetic field. The non-similar momentum, energy (temperature), and concentration (mass) relations have been derived utilizing non-dimensional variables. Emad et al. [7] evaluated the

consequences of a magnetic field (MHD) on the flow of nanomaterials in a boundary layer through a stretching plate/sheet. Various factors influencing the motion of nanofluid and particles are examined, particularly the alterations in the stretching sheet induced by an external magnetic field containing nanoparticles like Cu. MHD micropolar material flow through a porous heated/cooled deformable sheet with mixed convection are analyzed by Turkyilmazoglu [8]. Chen et al. [9] reported the numerical characteristics of MHD flow in the EU DEMO WCLL breeding blanket with the aspects of mixed convection.

In many engineering processes, the study of problems merging coupled heat and mass transport with chemical processes is important, and it has been generating a lot of attention recently. These processes are used in drying, energy transfer in wet cooling towers, surface evaporate in water bodies, and movement in desert coolers. Both homogeneous and heterogeneous are analyzed through chemical reactions, with homogeneous reactions occurring uniformly throughout a given phase, while heterogeneous reactions take place in specific regions or within phase boundaries. A reaction is considered first order if the rate is directly related to its concentration. The circulation of species with chemical reactions in boundary layer flows has wide-ranging applications in pollution investigation, fibrous insulating materials, oxidation process, and the materials synthesis, among others. Lu et al. [10] introduced a comprehensive model that couples heat and mass transport, and it is solved through numerical methods. The insights obtained from this model, both on a global and local scale, play a crucial role in enhancing our understanding of the transfer mechanisms, particularly highlighting the substantial impact of mass transfer within the pellet under conditions of low pressure and low permeability. These are significant phenomena that were overlooked by previous models. Aspects of heat and mass transport in a viscous nanomaterials through a porous flat sheet within a constant magnetic field is assessed by Arshad et al. [11]. The study incorporates factors such as Brownian motion, thermophoresis, and viscous dissipation. The governing relations are converted into standard nonlinear differential systems through suitable variables and are subsequently solved numerically in MATLAB utilizing the boundary value problem (BVP) scheme. Qayyum et al. [12] focused on addressing the influences of chemical species/reaction and nonlinear thermal radiative flow of a third-grade magneto nanomaterial towards a stretched sheet. The use of the Cattaneo-Christov double-diffusion model to examine the flow of Walters-B nanomaterial through an impermeable stretched wall was investigated by Hayat et al. [13]. The

study includes a thorough analysis of mass and heat transmission, taking into account variables like chemical reactions and heat generation/absorption.

In fluid dynamics, a location on the surface of an object is termed a stagnation point when the local fluid velocity is zero at that specific point. The stagnation pressure, characterized by the highest static pressure, is attained at this stagnation point. This concept finds relevance in various geometric and engineering applications, such as the leading edge of aircraft wings, the tips of high-speed submarines, missiles, and oil ships. Qayyum et al. [14] studied the aspects of MHD chemical reactive stagnation point flow of Walters-B nanomaterial in frame of Newtonian conditions. Bai et al. [15] studied dynamics of unsteady stagnation point oblique flow, along with heat and mass transport, is conducted for a generalized Oldroyd-B material over an oscillating plate. Chu et al. [16] explored the flow characteristics involving stagnation point and mixed convection of a viscoelastic micropolar liquid into a porous medium directed towards a stretchable plate, in view of a magnetic field.

1.2 Problem statement

In this work concentrates on the stagnation point of magnetic flow of viscous/Newtonian material through a permeable stretched plate in view of a first order chemical species/reaction. The homotopy analysis scheme (HAM) is utilized to formulate and solve analytically the governing systems for velocity (flow field), temperature (T) and concentration (C). The convergence analysis of the HAM solutions is demonstrated by both graphically and numerically. A comprehensive study exhibited the impacts of several variables/parameters on the dimensionless velocity (liquid flow field), temperature (T) and concentration (C) as well as the coefficient of skin friction and the local Nusselt and Sherwood numbers (rates heat and mass transfer) is carried out.

1.3 Aims and Objectives

1. MHD boundary layer flow are analyzed through a stretched sheet.
2. Governing equations are obtained through suitable transformations.
3. Resulting system are solved through homotopy analysis method.

Literature review and some basic preliminaries

2.1 Literature review

Section 2: Heat and mass transfer characteristics towards a stretched wall/plate in view of suction/blowing are reported by Gupta and Gupta [17]. Hsiao [18] reported the flow of stagnation point magneto nanomaterial with slip boundary on a stretching plate. MHD unsteady flow of boundary layer towards a shrinking sheet with the influence of radiation and heat sink/source are explored by Bhattacharyya [19]. Abel et al. [20] explored the Non- Newtonian materials for porous medium in view of convective heat and mass transport towards a stretched wall/surface. Hayat et al. [21] focused on the magnetic (MHD) heat transfer flow phenomena of a thirdgrade liquid towards a stretched wall with axisymmetric facets. Rashidi et al. [22] deliberated the entropy generation of magnetohydrodynamics (MHD) fluid flow towards a stretched rotating disk. Bhattacharyya et al. [23] was looked at the stagnation point flow of magnetic material through a stretched wall with suction/blowing. Ramesh et al. [24] scrutinized the non-uniform source/sink with MHD (magnetohydrodynamics) flows of a permeable stretching plate. Impact of chemical species on the magneto-micropolar material flow with heat and mass transfer was studied by Das [25]. Chakraborty and Mazumdar [26] considered MHD flow of viscous materials through a stretched wall. Qayyum et al. [27] discussed the MHD chemical reactive flow of Jeffrey nanomaterials along a nonlinear stretched wall with nonlinear mixed convection. Dash et al. [28] analyzed the stagnation point flow with various aspects along a stretching/shrinking wall in frame of numerical approach. MHD (magneto hydrodynamics) radiative stagnation point flow of a nanomaterial through a stretched wall are scrutinized by Jalilpour et al. [29]. Rashidi et al. [30] discussed the MHD radiative of nanomaterial through a stretched plate with buoyancy forces. Sheikholeslami et al. [31] analyzed the features of MHD (magneto hydrodynamics) heat transfer flow of nanoliquid with radiation features. Pop et al. [32] evaluated the radiative stagnation point of oblique flow through a stretched wall with various aspects. Characteristics of MHD (magneto hydrodynamics) flow of heat transfer towards a stretching horizontal cylinder in frame of suction/injection with heat sink/source was studied by Elbashbeshy et al. [33]. Sharma and Singh [34] explored the features of MHD material flow near a stagnation point towards a stretched wall with thermal conductivity in variable facets. Xu et al. [35] reported unsteady flow in a nano-material film through a stretched sheet. Sheikholeslami et al [36] studied the MHD radiative flow of nano materials flow and heat transfer by means of two phase model. Features of radiation and axisymmetric MHD flow of Caisson fluid towards a porous surface are explained by Mahabaleshwar et al. [37]. MHD chemical reactive flow of nanofluid flow towards an

absorbent sheet are discussed by Dey and Mukhopadhyay [38]. MHD flow of non-Newtonian fluid with thermophoresis and Brownian aspects are described by Qayyum et al. [39]. Nadeem et al. [40] explored the numerical results of hybrid nano-fluid in frame of semi-annular channel with heat transfer. MHD micropolar material flow through a porous heated/cooled deformable sheet with mixed convection are analyzed by Turkyilmazoglu [41]. Sheikholeslami et al. [42] reported the features of magnetic field in unsteady nanomaterials flow in frame of Buongiorno model. Vajravelu [43] investigated the flow features of a viscous material towards a nonlinearly stretching plate. Utilizing a different similarity transformation from the one used for the linearly expanding sheet, the systems of conservation of mass, momentum, energy and concentration that control the fluid flow and heat transfer. Heat and mass transport in view of suction/blowing towards the stretching surface was discussed by Gupta and Gupta [44]. Unsteady natural convection flow of nanomaterails through a vertical flat surface with radiation aspects are reported by Turkyilmazoglu and Pop [45]. Rajput et al. [46] reported the unsteady nonlinearly stretching sheet with the flow of nanomaterials in frame of variable properties. Mabood [47] investigated the chemical reactive stagnation point flow on the stretching plate in view of magnetic field (MHD).

2.2 Basic definitions

2.2.1 Fluid

A fluid material that deforms continuously when the applied it the shear forces. Examples of fluids are liquids and gases.

Liquid

The liquid is a type of fluid which do not a specific shape. For examples, water, ink and honey etc.

Gas

The gas is a type of fluid which also do not a specific shape and size. For examples, carbon dioxide, oxygen, nitrogen, methane etc.

2.2.2 Fluid mechanics

The types of continuum mechanics which analyzed the fluid properties either in motion or in rest is defined as fluid mechanics. Here further classified into three categories.

Statics fluid

The fluids properties studies in frame of rest.

Kinematics fluid

The fluids properties studies in frame of motion.

Dynamics fluid

The fluid motion studies due to effect of forces.

2.2.3 Stress

Stress is defined by an average force of fluid particles acting on the deformable body with the unit surface area.

Shear stress

Shear stress occurs when a force occurs orthogonal to the unit area of the deformable body.

Normal stress

When force acts normal to the unit surface area in a deformable object, the stress is regarded to be normal.

2.2.4 Viscosity

Viscosity is the ability of the liquid material that resist the flow. There are two types of viscosity

Dynamic viscosity

The relation between shear stress and velocity gradient is referred to dynamic viscosity. Symbolically its stands for μ. Mathematically

$$\mu = \tau / \frac{\partial y}{\partial u}. \tag{2.1}$$

In system SI its unit and dimension are $kg / m.s$ and $[ML^{-1}T^{-1}]$ respectively.

Kinematic viscosity

The relation between dynamic viscosity and fluid density is referred to kinematic viscosity. Symbolically its stands for ν. Mathematically

$$\nu = \frac{\mu}{\rho}. \tag{2.2}$$

Its unit m^2 / s and dimension $[L^2T^{-1}]$ in SI system.

2.2.5 Viscous Fluids

A fluid characterizes as a viscous fluid if its viscosity may change or uniform due to different type of stresses. These fluids can be subdivided as follows:

Newtonian fluid

The fluids in which shear stress and velocity gradient are directly proportional but in a linear manner. Here viscosity is uniform under the shear stress. Examples for Newtonian fluid are water, sugar solvents, milk, mineral and ethyl alcohol.

Non-Newtonian fluid

Non-Newtonian liquids/fluids are described as fluid materials that do not adhere to Newton's law of viscosity. Mathematically

$$\tau_{yx} = \eta \frac{du}{dy} \quad \text{where} \quad \eta = k\left(\frac{du}{dy}\right)^{n-1} \text{ and } n \neq 1, \tag{2.3}$$

where n, η and k stands for flow behavior index, apparent viscosity and consistency index respectively. Paints, tooth paste, ketchup, blood and polymer solutions etc. are the examples of non-Newtonian materials.

2.2.6 Magnetohydrodynamics

Magnetohydrodynamics is the study of the dynamical matter moving in an electromagnetic field. Magnetic field makes the stream lines smooths out which consequences the thinner boundary layer. It can also be applied to control efficiently the transport of heat and mass in the boundary layer flow field of innumerable fluid materials. Magnetic parameter also called Hartmann number (M).

Maxwell's relations

The differential type of Maxwell's relations are given by

$$\text{div}\,\mathbf{E}_{ap} = \nabla.\mathbf{E} = \frac{\rho}{\varepsilon_0}, \quad \text{Guass's law} \tag{2.4}$$

$$\text{div}\mathbf{B} = \nabla.\mathbf{B} = 0, \quad \text{Solenoidal nature of } \mathbf{B} \tag{2.5}$$

$$\text{curl}\,\mathbf{E}_{in} = \nabla \times \mathbf{E} = -\left(\frac{\partial \mathbf{B}}{\partial t}\right), \quad \text{Faraday's theory} \tag{2.6}$$

$$\text{curl}\mathbf{B} = \nabla \times \mathbf{B} = \mu_0\left(\mathbf{J} + \varepsilon_0 \frac{\partial \mathbf{E}_{ap}}{\partial t}\right), \quad \text{Ampere Maxwell equation} \tag{2.7}$$

These are the basic equations in electromagnetism which relates electric and magnetic field. We derive the term for magnetohydrodynamic and in Joule heating case from above four equations. In these equations $\left(\mathbf{E}_{ap}, \mathbf{E}_{in}\right)$ represents applied and induced electric field, $\left(\rho, J\right)$ corresponds to charge and current densities, ε_0 is the permittivity of the free space, $\mathbf{B}$ represents the sum of applied and induced magnetic field and μ_0 represents the magnetic permeability.

Lorentz force

Lorentz force is the force on a point charge q due to joint impact of electric and magnetic fields. If an external magnetic field $\mathbf{B}$ is present, $\mathbf{V}$ is the velocity of moving fluid and σ is the electrical conductivity then Lorentz force is defined by:

$$\mathbf{F} = q(\mathbf{E}_{ap} + \mathbf{V} \times \mathbf{B}). \tag{2.8}$$

Current density

It characterizes the quantity of an electric current passing through a unit area cross sectional (of a surface) at a specified region. Symbolically denoted by $\mathbf{J}$. Mathematically

$$\mathbf{J} = \sigma(\mathbf{E}_{ap} + \mathbf{V} \times \mathbf{B}). \tag{2.9}$$

2.2.7 Chemical reaction

It is defined as a chemical change in one or more substances to produce new substances.

2.2.8 Stagnation point

A stagnation point is a place in the flow field when there is no motion in the fluid is known as a stagnation point if the local velocity of fluid is zero at that point.

2.3 Non-dimensionalize parameters

2.3.1 Reynold number

Ratio of inertial and viscous forces are defined as Reynold number. Mathematically it can be expressed by

$$\mathrm{Re} = \frac{\text{Inertial forces}}{\text{Viscous forces}} \propto \frac{\rho u \frac{\partial u}{\partial x}}{\mu \frac{\partial^2 u}{\partial x^2}} = \frac{\rho u x}{\mu} = \frac{ux}{\nu}, \tag{2.10}$$

where ρ stands for density, μ stands for dynamic viscosity, u and x stands for characteristics velocity and distance.

2.3.2 Prandtl number

Prandtl number (Pr) is the definition of the ratio between thermal diffusivity and kinematic viscosity. Mathematically

$$\mathrm{Pr} = \frac{\nu}{\alpha}, \tag{2.11}$$

where ν and α stands for kinematic viscosity and thermal diffusivity.

2.3.3 Schmidt number

Schmidt number (Sc) is the definition of the ratio between mass diffusivity and kinematic viscosity. Mathematically

$$Sc = \frac{\nu}{D}, \tag{2.12}$$

where D stands for mass diffusivity.

2.3.4 Hartmann number

Hartmann number is used to express a relation among electromagnetic and viscous forces. It is defined as electromagnetic to viscous forces ratio. Mathematically

$$M^2 = \frac{\sigma B_0^2}{\rho a}, \tag{2.13}$$

where σ stands electrical conductivity, B_0 stands for applied magnetic field, ρ stands for fluid density and a stands for positive constant.

2.3.5 Skin friction coefficient

Skin friction is the amount of friction that occurs when fluid moves across a surface. It happens between the fluid and the surface, which tends to slow the fluid's motion. Mathematically

$$C_f = \frac{\tau_w}{\rho U^2 / 2}, \tag{2.14}$$

where τ_w stands for shear stress at the wall, ρ stands for density and U stands for free-stream velocity.

2.3.6 Nusselt number

Nusselt number is the dimensionless heat transfer measurement which provides a measure of heat transfer of the convective and conductive ratio across the boundary and can be stated as

$$Nu_L = \frac{\text{heat convective transfer coefficient}}{\text{heat conductive transfer coefficient}}. \tag{2.15}$$

Now heat transfer by convection is $\left(h\Delta T\right)$ and by conduction is $\left(k\Delta T / L\right)$. So Nusselt number becomes

$$Nu_L = \frac{h\Delta T}{k\Delta T / L} = \frac{hL}{\kappa}, \tag{21.6}$$

where h, L and κ stands for convective heat transfer, characteristic length and thermal conductivity of the material.

2.3.7 Sherwood number

Sherwood number is the amount of convective and diffusive mass transfers ratio. Mass transfer by convection and diffusion is given by $K\left(C_w - C_\infty\right)$ and $D\left(C_w - C_\infty\right)/L$ respectively i.e.,

$$Sh = \frac{K\Delta C}{D\Delta C / L} = \frac{KL}{D}, \tag{2.17}$$

where K and D stands for mass transfer rate and diffusion coefficient.

2.4 Conservation laws

2.4.1 Law of mass conservation

This relation is obtained by utilizing the theory of mass conservation which is expressed as the mass can cannot be created nor be destroyed. Mathematically the continuity equation seems like that when there are no sources or sinks

$$\frac{\partial \rho}{\partial t} + \nabla.(\rho \mathbf{V}) = 0, \tag{2.18}$$

where ρ stands for density, t stands for time and $\mathbf{V} = (u, v, w)$ stands for liquid velocity. For an incompressible fluid, the continuity is obtained as

$$\nabla.\mathbf{V} = 0. \tag{2.19}$$

2.4.2 Law of momentum conservation

Law of conservation momentum is obtained through Navier-Stokes systems which can be defined as

$$\rho \frac{d\mathbf{V}}{dt} = \nabla.\tau + \rho \mathbf{b}, \tag{2.20}$$

where τ and $\mathbf{b}$ stands for Cauchy stress tensor and body forces for incompressible fluid is

$$\tau = -p\mathbf{I} + \mathbf{A}_1, \tag{2.21}$$

in which p, $\mathbf{I}$ and $\mathbf{A}_1 = \nabla.\mathbf{V} + \left(\nabla.\mathbf{V}\right)^t$ stand for pressure, identity tensor and first Rivlin-Erickson tensor respectively.

2.4.3 Law of energy conservation

Law of energy conservation is obtained through 1st law of thermodynamics, which defines that heat added to system is equal to upsurge in temperature of the system and work done by the system. Using this law energy relation can be defined as

$$\rho c_p \frac{dT}{dt} = tr\left(\tau.\ \left(\text{grad}\mathbf{V}\right)\right) - \text{div}\mathbf{q}, \tag{2.22}$$

where T, c_p and $\mathbf{q}$ stands for temperature, specific heat and vector of heat flux described as

$$\mathbf{q} = -\kappa \nabla T, \tag{2.23}$$

where κ sights for material (fluid) thermal conductivity and negative sign appears that of heat flux vector at any point on surface remain normal to the surface/sheet and point through diminishing temperature.

2.4.4 Law of concentration conservation

Law of concentration conservation is obtained through Fick's first and second law which can be defined as

$$\frac{dC}{dt} = D\nabla^2 C. \tag{2.24}$$

2.5 Homotopy analysis method (HAM)

In order to elucidate the non-linear problems, Liao [48] proposed a method which is known as homotopy analysis technique (HAM). We consider the following differential relation

$$N\left[u\left(x\right)\right] = 0, \tag{2.25}$$

where x (independent variable), N (non-linear operator) and $u\left(x\right)$ (unknown function). The zeroth-order deformation relation is

$$\left(p-1\right)\mathbf{L}\left[\widehat{u}\left(x;p\right) - u_0\left(x\right)\right] = -p\hbar N\left[\widehat{u}\left(x;p\right)\right], \tag{2.26}$$

in which $u_0\left(x\right)$, $\mathbf{L}$, $\hbar$, $p \in \left[0,1\right]$ denotes initial solution, auxiliary linear operator, auxiliary variable, embedding variable and $\widehat{u}\left(x;p\right)$ is unknown function of x and p.

For $p = 0$ and $p = 1$, One obtain

$$\widehat{u}(x;0)=u_0(x) \text{ and } \widehat{u}(x;1)=u(x), \tag{2.27}$$

when p goes from 0 to 1, $\widehat{u}(x;p)$ (solution) contrasts from $u_0(x)$ (initial solution) to $u(x)$ (final solution). Through Taylor series relation one can write

$$\widehat{u}(x;p)=u_0(x)+\sum_{n=1}^{\infty}u_n(x)\,p^n,\;\; u_n(x)=\frac{1}{n!}\frac{\partial^n\widehat{u}(x;p)}{\partial p^n}\bigg|_{p=0}, \tag{2.28}$$

when $p=1$, we get

$$u(x)=u_0(x)+\sum_{n=1}^{\infty}u_n(x). \tag{2.29}$$

Differentiating Eq. (2.26) (zeroth-order deformation relation) n-time with respect to p, then dividing by $n!$ and finally obtaining $p=0$, we develop the n-th order deformation relation

$$\mathbf{L}\left[u_n(x)-\chi_n u_{n-1}(x)\right]=\hbar\mathbf{R}_n(x), \tag{2.30}$$

$$\mathbf{R}_n(x)=\frac{1}{(n-1)!}\frac{\partial^n N\left[\widehat{u}(x;p)\right]}{\partial p^n}\bigg|_{p=0}, \tag{2.31}$$

with

$$\chi_n=\begin{cases}0, & n\le 1\\ 1, & n>1\end{cases}. \tag{2.32}$$

MHD viscous fluid flow towards a stretched surface

This Section 3 addresses the (2D) two-dimensional boundary layer of magnetic flow of viscous/Newtonian fluid in frame of heat transfer characteristics over stretchable surface is analyzed. Constant temperature is imposed at the surface of sheet. Suitable variables are utilized to acquire the nonlinear ordinary differential (ODEs) systems. Analytical solutions of governing system is acquired utilizing HAM. The impact of sundry parameters are presented through graphs and tabulated values. Coefficient of skin friction (C_{fx}) and local Nusselt number (Nu_x) (heat transfer rate) are computed and analyzed numerically.

3.1 Mathematical description

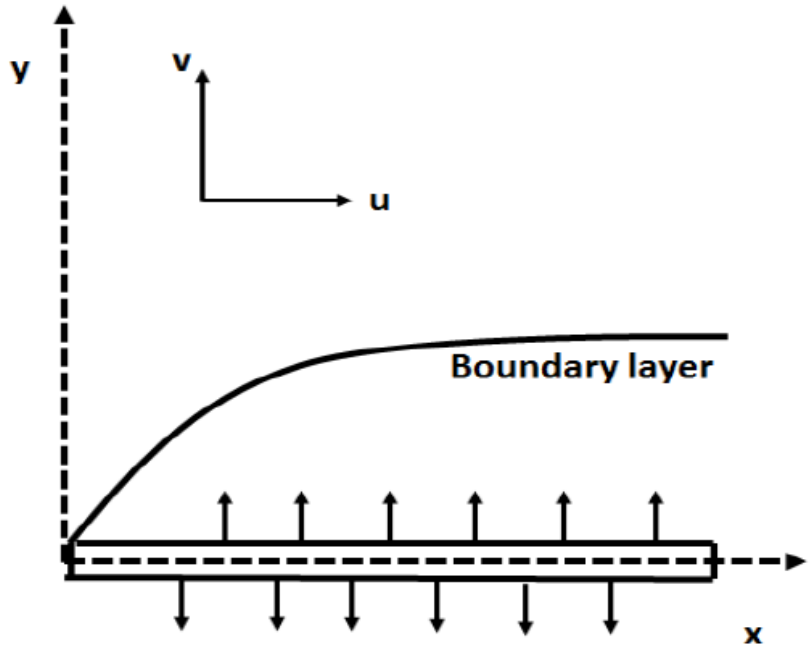

Fig. 3.1: Diagram of Physical model.

Here we analyze the magnetic (MHD) flow of a viscous/Newtonian incompressible liquid past towards a flat heated plate that corresponds with the plane at the *x*-axis $y=0$. The material flow is limited to $y>0$. The governing systems for such nature of flow are stated as

$$\frac{\partial u}{\partial x}+\frac{\partial v}{\partial y}=0, \tag{3.1}$$

$$u\frac{\partial u}{\partial x}+v\frac{\partial u}{\partial y}=\nu\frac{\partial^2 u}{\partial y^2}\ -\frac{\sigma B_0^2}{\rho}u\ , \tag{3.2}$$

$$u\frac{\partial T}{\partial x}+v\frac{\partial T}{\partial y}=\frac{\kappa}{\rho c_p}\frac{\partial^2 T}{\partial y^2}, \tag{3.3}$$

$$\begin{aligned} u(x,0)=ax,\ v(x,0)=0,\ T(x,0)=T_w,\\ u(x,\infty)=0,\ v(x,\infty)=0,\ T(x,\infty)=T_\infty. \end{aligned} \tag{3.4}$$

We define the transformations

$$\begin{aligned} u=axf'(\eta),\ v=-(a\nu)^{\frac{1}{2}}\ f(\eta),\ \psi=(a\nu)^{\frac{1}{2}}\ xf(\eta),\\ \eta=\left(\frac{a}{\nu}\right)^{\frac{1}{2}}\ y,\ \theta=\frac{T-T_\infty}{T_w-T_\infty}. \end{aligned} \tag{3.5}$$

Here (u,v) corresponds to components of velocity in (x,y) directions, T views for fluid temperature, κ stands for material thermal conductivity, ρ views for fluid density, ν views for kinematic viscosity, c_p views for specific heat, B_0 views for applied magnetic field normal to the direction of flow, a views for positive constant.

Using Eq. (3.5) on Eq. (3.1-3.4), we get the resultant systems and boundary conditions

$$f'''-f'^2+ff''-M^2f'=0, \tag{3.6}$$

$$\theta'' + \Pr \theta' f = 0, \tag{3.7}$$

with

$$\begin{aligned} f(0) = 0, \;\; f'(0) = 1, \;\; \theta(0) = 1, \\ f'(\infty) \to 0, \;\; \theta(\infty) \to 0. \end{aligned} \tag{3.8}$$

where $M = \frac{\sigma B_0^2}{\rho a}$ (Hartmann number) and $\Pr = \frac{\mu c_p}{\kappa}$ (Prandtl number).

The relations of C_{fx} (coefficient of skin friction) and Nu_x (heat transfer rate) are expressed by

$$C_{fx} = \frac{2\tau_{xy}\big|_{y=0}}{\rho U_w^2}, \; Nu_x = \frac{x q_w}{\kappa\left(T_w - T_\infty\right)}. \tag{3.9}$$

Using Eq. (3.5) in Eq. (3.10), we obtain

$$\left(\frac{\mathrm{Re}_x}{2}\right)^{1/2} C_{fx} = -f''(0), \; \left(\frac{\mathrm{Re}_x}{2}\right)^{-1/2} Nu_x = -\theta'(0), \tag{3.10}$$

where $q_w = -\kappa\left(\frac{\partial T}{\partial y}\right)_{y=0}$ (wall heat flux), $\tau_{xy} = -\mu\left(\frac{\partial u}{\partial y}\right)_{y=0}$ (wall shear stress) and $\mathrm{Re}_x = \sqrt{\frac{a}{\nu}}x$ (local Reynold number).

3.2 Homotopic procedure

We take initial solutions and linear operators are expressed as

$$f_0(\eta) = 1 - \exp(-\eta), \; \theta_0(\eta) = \exp(-\eta), \tag{3.11}$$

$$\mathbf{L}_f\left(f\right) = f''' - f', \; \mathbf{L}_\theta\left(\theta\right) = \theta'' - \theta, \tag{3.12}$$

with

$$\mathbf{L}_f\left\{\tau_1^* + \tau_2^* \exp(\eta) + \tau_3^* \exp(-\eta)\right\} = 0, \tag{3.13}$$

$$\mathbf{L}_\theta\left\{\tau_4^* \exp(\eta) + \tau_5^* \exp(-\eta)\right\} = 0, \tag{3.14}$$

where τ_i^* $(i=1-5)$ shows the unknown constants.

3.2.1 Deformation statements of zeroth-order

$$(p-1)\mathbf{L}_f\left[f(\eta;p)-f_0(\eta)\right]=-p\hbar_f H_f \mathbf{N}_f\left[f(\eta;p)\right], \tag{3.15}$$

$$(p-1)\mathbf{L}_\theta\left[\hat{\theta}(\eta;p)-\theta_0(\eta)\right]=-p\hbar_\theta H_\theta \mathbf{N}_\theta\left[\hat{\theta}(\eta;p), f(\eta;p)\right], \tag{3.16}$$

$$f(0;p)=0,\quad f'(0;p)=1 \text{ and } f'(\eta;p)\to 0 \text{ as } \eta\to\infty, \tag{3.17}$$

$$\hat{\theta}(0;p)=1 \text{ and } \hat{\theta}(\eta;p)\to 0 \text{ as } \eta\to\infty, \tag{3.18}$$

$$\mathbf{N}_f\left[f(\eta,p)\right]=f'''-f'^2-M^2 f'+f f'', \tag{3.19}$$

$$\mathbf{N}_\theta\left[\hat{\theta}(\eta;p), f(\eta;p)\right]=\hat{\theta}''+\Pr\hat{\theta}' f, \tag{3.20}$$

in which $\left(\mathbf{N}_f,\mathbf{N}_\theta\right)$ and $\left(\hbar_f,\hbar_\theta\right)$ are the non-linear operators and non-zero auxiliary variables respectively, p is an embedding variable. For $p=0$ and 1 one yields

$$f(\eta;0)=f_0(\eta),\quad f(\eta;1)=f(\eta), \tag{3.21}$$

$$\hat{\theta}(\eta;0)=\theta_0(\eta),\quad \hat{\theta}(\eta;1)=\theta(\eta), \tag{3.22}$$

3.2.2 Deformation systems of nth-order

$$\mathbf{L}_f\left[\, f_n(\eta)-\chi_n f_{n-1}(\eta)\,\right]=\hbar_f \mathbf{R}_n^f(\eta), \tag{3.23}$$

$$\mathbf{L}_\theta\left[\, \theta_n(\eta)-\chi_n \theta_{n-1}(\eta)\,\right]=\hbar_\theta \mathbf{R}_n^\theta(\eta), \tag{3.24}$$

$$f_n(0)=0,\ f_n'(0)=1 \text{ and } f_n'(\eta)\to 0 \text{ as } \eta\to\infty, \tag{3.25}$$

$$\theta_n(0)=1 \text{ and } \theta_n(\eta)\to 0 \text{ as } \eta\to\infty, \tag{3.26}$$

$$\mathbf{R}_n^f(\eta)=f_{n-1}'''(\eta)-M^2 f_{n-1}'(\eta)-\sum_{k=0}^{n-1}\left(f_{n-1-k}' f_k'+f_{n-1-k} f_k''\right), \tag{3.27}$$

$$\mathbf{R}_n^\theta(\eta)=\theta_{n-1}''(\eta)+\Pr\sum_{k=0}^{n-1}\theta_k' f_{n-1-k}, \tag{3.28}$$

$$\chi_n=\begin{cases}0, & \text{when } n\le 1,\\ 1, & \text{when } n>1.\end{cases} \tag{3.29}$$

If we take values of p through 0 to 1 then $f(\eta;p)$ and $\widehat{\theta}(\eta;p)$ change from $f_0(\eta)$ and $\theta_0(\eta)$ (initial results) to $f(\eta)$ and $\theta(\eta)$ (final results) respectively. With Taylor series, we've gained

$$f(\eta;p)=f_0(\eta)+\sum_{n=1}^{\infty}p^n f_n(\eta) \text{ with } f_n(\eta)=\frac{1}{n!}\frac{\partial^n f(\eta;p)}{\partial p^n}\bigg|_{p=0}, \tag{3.30}$$

$$\widehat{\theta}(\eta;p)=\theta_0(\eta)+\sum_{n=1}^{\infty}p^n\theta_n(\eta)\ \text{ with }\ \theta_n(\eta)\ =\ \frac{1}{n!}\frac{\partial^n\widehat{\theta}(\eta;p)}{\partial p^n}\bigg|_{p=0}, \tag{3.31}$$

The suitable values of $\hbar_f$ and $\hbar_\theta$ (auxiliary variables) in above systems are preferred in such a way that we achieve convergent solution at $p=1$. Therefore

$$f(\eta)=\ f_0(\eta)+\sum_{n=1}^{\infty}f_n(\eta), \tag{3.32}$$

$$\theta(\eta)=\theta_0(\eta)+\sum_{n=1}^{\infty}\theta_n(\eta). \tag{3.33}$$

Regarding the special solutions $\left(f_n^*,\ \theta_n^*\right)$, the general solutions are

$$f_n(\eta)=\ f_n^*(\eta)+\tau_1^*+\tau_2^*\exp(\eta)+\tau_3^*\exp(-\eta), \tag{3.34}$$

$$\theta_n(\eta)=\theta_n^*(\eta)+\tau_4^*\exp(\eta)+\tau_5^*\exp(-\eta), \tag{3.35}$$

where $\tau_i\,(i=1-5)$ are constants and can be found

$$\begin{aligned}&\tau_1^*=-\tau_3^*-\ f_n^*(0),\ \tau_3^*=\frac{\partial f_n^*(\eta)}{\partial\eta}\bigg|_{\eta=0},\\&\tau_5^*=-\theta_n^*(\eta)\big|_{\eta=0},\ \tau_2^*=\tau_4^*=0.\end{aligned} \tag{3.36}$$

3.3 Homotopic convergence

We know that the homotopic solutions contains $\hbar_f$ and $\hbar_\theta$ (auxiliary variables). These variables determine the homotopic convergence solutions. The relevant $\hbar$-curves have been strategized in the Figs. 3.2 and 3.3. It has been observed that the adequate ranges of $\hbar_f$ and $\hbar_\theta$ are $-1.9\le\hbar_f\le-0.1$ and $-1.9\le\hbar_\theta\le-0.3.$ Table 3.1 depicts the convergence of homotopic solution

for the function $\left(f(\eta), \theta(\eta) \right)$ by adjusting particular values of $\hbar_f$ and $\hbar_\theta$. It is observed that 11^{th} order of approximation is must for the convergence of function $f(\eta)$ whereas 28^{th} order of approximation is must for function $\theta(\eta)$.

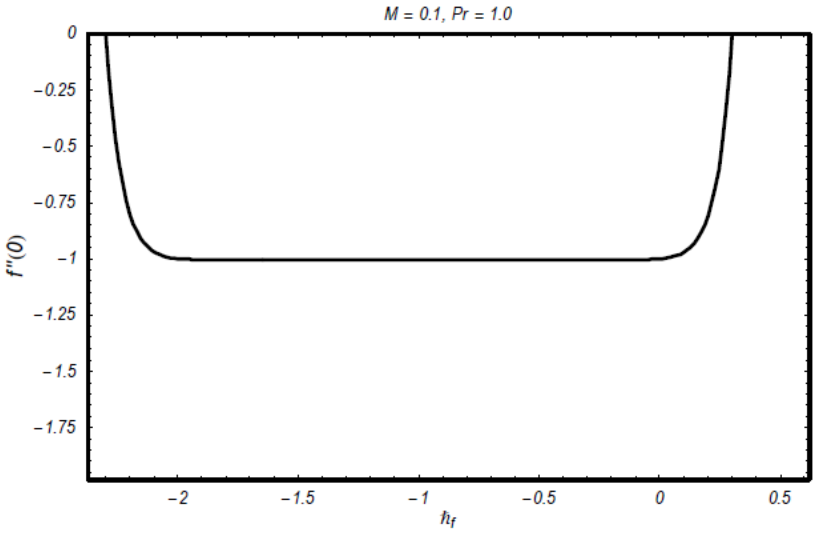

Fig. 3.2: $\hbar$ -curve for $f''(0)$.

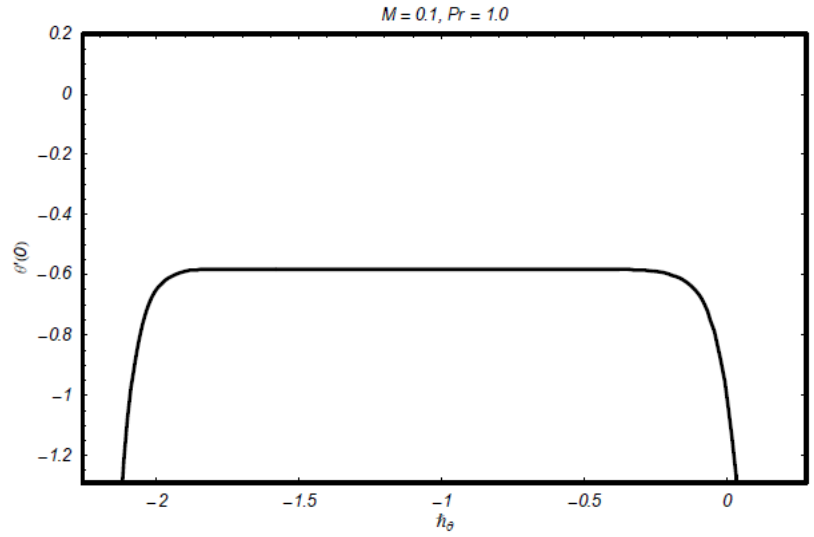

Fig. 3.3: $\hbar$ -curve for $\theta'(0)$.

Table 3.1: Homotopic solutions converges for $M = 0.1$ and $\Pr = 1.0$.

Order of approximations	$-f''(0)$	$-\theta'(0)$
1	1.00250	0.83333
5	1.00483	0.62143
10	1.00498	0.58685
11	1.00499	0.58510
15	1.00499	0.58202
20	1.00499	0.58116
25	1.00499	0.58099
28	1.00499	0.58096
35	1.00499	0.58096

3.4 Graphical description

Following the homotopy analysis system describe in previous section, results are acquired for various values of M (Hartmann number) and $\Pr$ (Prandtl number) on the $f'(\eta)$ (velocity) and $\theta(\eta)$ (temperature). Graphs with respect to these parameter are plotted through Mathematica software and shown in Figs. 3.4-3.6. Fig. 3.4 depict the influence of M on $f'(\eta)$. It is observable that the $f'(\eta)$ decreases with M. For larger M the rate of transport reduces due to increase in Lorentz force. Aspects of M on $\theta(\eta)$ (temperature field) is sketched in Fig. 3.5. Here $\theta(\eta)$ enhances for larger M. Fig. 3.6 is reported for the impact of $\Pr$ on $\theta(\eta)$. Here we revealed that

both $\theta(\eta)$ and thickness of associated boundary layer diminishes with the increment of $\Pr$. Table 3.2 is interpreted to skin friction coefficient. Here exposed that the skin friction coefficient improves in excess of the (M) Hartmann number. The heat transfer analysis under the consideration of physical parameters encountered in Table 3.3. It is interesting to see that heat transfer rate enhances by increasing Prandtl number and it decreases with the enhancement of Hartmann number.

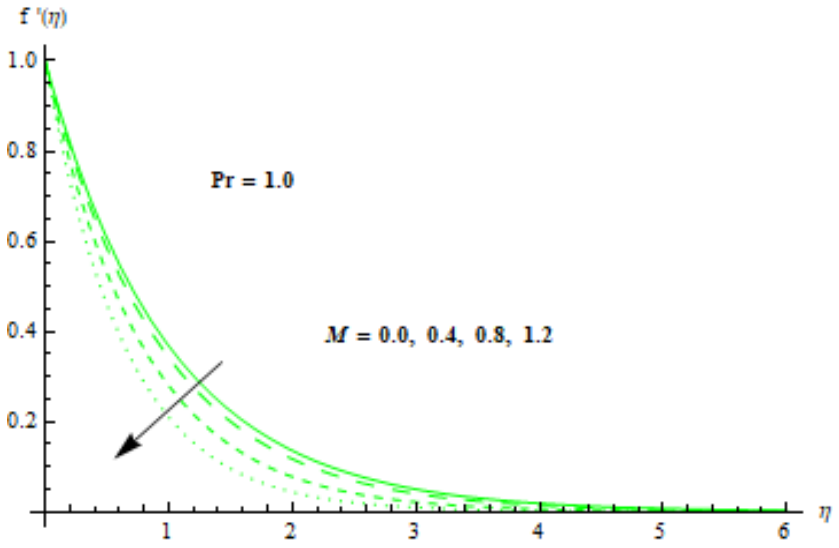

Fig. 3.1: M effects on $f'(\eta)$.

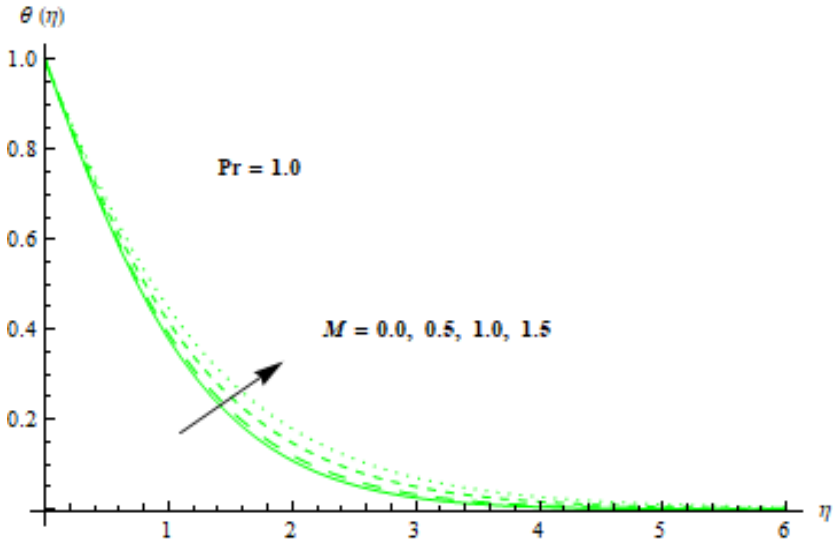

Fig. 3.2: M effects on $\theta(\eta)$.

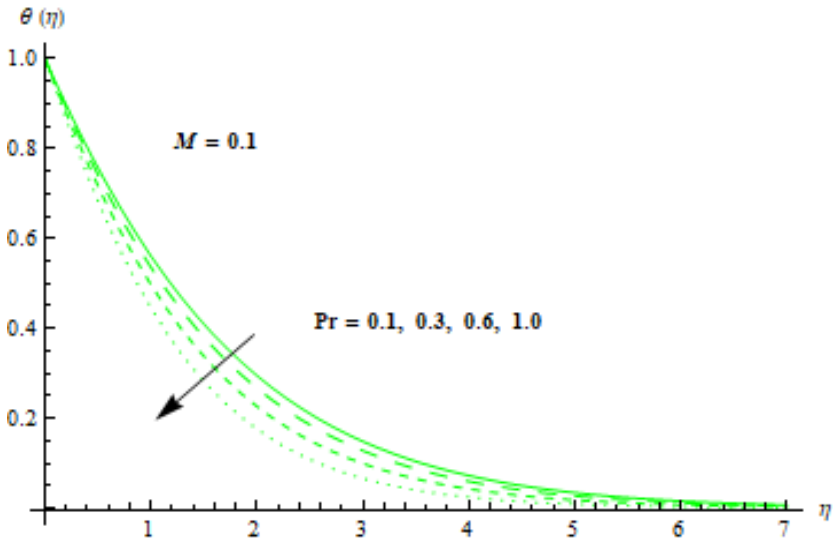

Fig. 3.3: $\Pr$ effects on $\theta(\eta)$.

Table. 3.2: Numerical solutions of $\left(\frac{\mathrm{Re}}{2}\right)^{1/2} C_{fx}$ (skin friction coefficient) for M .

M	$\left(\frac{\mathrm{Re}}{2}\right)^{1/2} C_{fx}$
0.1	1.418
0.5	1.565
0.8	1.664

Table. 3.3: Numerical solutions of $\left(\frac{\mathrm{Re}}{2}\right)^{-1/2} Nu_x$ (local Nusselt number) for M and Pr .

M	Pr	$\left(\frac{\mathrm{Re}}{2}\right)^{-1/2} Nu_x$
0.1		1.118
0.5		1.079
1.0		1.040
0.1	1.0	1.065

	1.5	1.520
	2.0	1.685

3.5 Closing remarks

In this chapter, we analyzed two-dimensional steady magneto-hydrodynamic (MHD) boundary layer of (Newtonian) viscous fluid flow towards a stretched wall. The key consequences are

- Action of M on the $f'(\eta)$ (velocity field) which causes velocity decreases.
- Same behavior of temperature field and its thickness layer for high $\Pr$.
- Opposite impact of $\left(\frac{\mathrm{Re}}{2}\right)^{-1/2} Nu_x$ (Nusselt Number) for increasing of M and $\Pr$.

Chemical reactive stagnation point flow of viscous fluid with magnetic field

In This Section 4 concentrates the steady magnetohydrodynamic (MHD) stagnation point flow of viscous liquid through heat and mass transport. The fluid flow is generated by a permeable stretched wall containing chemical species. The transformation technique utilizes similarity variables to simplify the nonlinear partial differential systems for flow field into ordinary differential systems. Convergent homotopic solutions are analyzed for the resulting nonlinear systems. Convergence interval is determined. A detailed study shows the impact of various variables on the dimensionless velocity (flow field), temperature, concentration as well as the coefficient of skin-friction (C_{fx}) and the local Nusselt (Nu_x) and Sherwood (Sh_x) numbers is showed.

4.1 Formulation of the problem

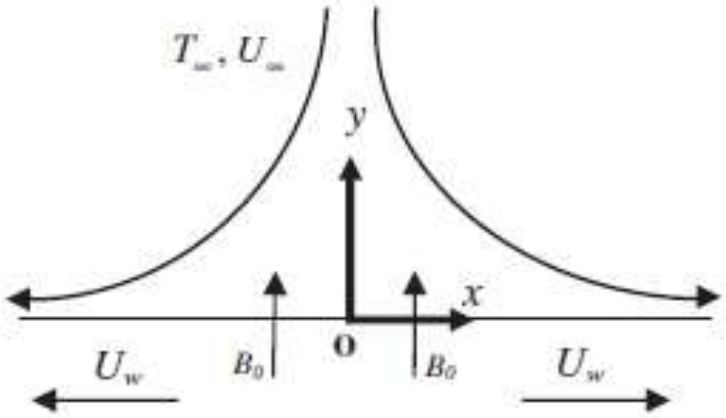

Fig. 4.1: Physical sketch.

The two-dimensional (2D) steady flow of a viscous material toward a permeable stretched plate with a chemical species/reaction and stagnation point flow are considered. Applied along y-aixs, a uniform transverse magnetic field of intensity B_0 is seen in Fig. 4.1. The fluid that conducts electricity and the produced magnetic field are disregarded. Assumed that $U_w(x) = ax$ and $U_\infty(x) = bx$ correspond to the stretching and free stream velocities, respectively, at the distance x as of the stagnation point. Temperature and concentration are sustained at the suggested constant values T_w, C_w, correspondingly at the surface. For viscous incompressible flow, constitutive equations are defined as

$$\frac{\partial u}{\partial x} + \frac{\partial v}{\partial y} = 0, \tag{4.1}$$

$$u\frac{\partial u}{\partial x} + v\frac{\partial u}{\partial y} = \nu\frac{\partial^2 u}{\partial y^2} + U_\infty\frac{\partial U_\infty}{\partial x} - \frac{\sigma}{\rho}B_0^2(U_\infty - u), \tag{4.2}$$

$$u\frac{\partial T}{\partial x}+v\frac{\partial T}{\partial y}=\frac{\kappa}{\rho c_p}\frac{\partial^2 T}{\partial y^2}, \tag{4.3}$$

$$u\frac{\partial C}{\partial x}+v\frac{\partial C}{\partial y}=D\frac{\partial^2 C}{\partial y^2}-R(C-C_\infty), \tag{4.4}$$

$$\begin{aligned} &u(x,y)\big|_{y=0}=U_w(x)=ax, v(x,y)\big|_{y=0}=v_w, T(x,y)\big|_{y=0}=T_w, C(x,y)\big|_{y=0}=C_w,\\ &u(x,y)\big|_{y\to\infty}=U_\infty(x)=bx, T(x,y)\big|_{y\to\infty}=T_\infty, C(x,y)\big|_{y\to\infty}=C_\infty, \end{aligned} \tag{4.5}$$

where (u,v) corresponds to velocity components in (x,y) directions, ρ the liquid density, ν the kinematic viscosity, R the reaction rate of solute, σ the electrical conductivity of liquid, c_p the specific heat, κ the material/fluid thermal conductivity, D the mass diffusion coefficient, T and C the liquid temperature and concentration, T_∞ and C_∞ the ambient temperature and concentration of fluid.

Now we define the transformations as follows

$$\begin{aligned} &u=axf'(\eta),\ v=-(a\nu)^{\frac{1}{2}}f(\eta),\ \psi=(a\nu)^{\frac{1}{2}}xf(\eta),\\ &\eta=\left(\frac{a}{\nu}\right)^{\frac{1}{2}}y,\ \theta(\eta)=\frac{T-T_\infty}{T_w-T_\infty},\ \phi(\eta)=\frac{C-C_\infty}{C_w-C_\infty}. \end{aligned} \tag{4.6}$$

Using Eq. (4.6) in Eqs. (4.1-4.5), we acquire the following resultant systems and boundary conditions

$$f'''-f'^2+ff''+\varepsilon^2+M(\varepsilon-f')=0, \tag{4.7}$$

$$\theta''+\Pr\theta' f=0, \tag{4.8}$$

$$\phi"-Sc(\gamma\phi-f\phi')=0, \tag{4.9}$$

with

$$\begin{aligned} f(0) &= f_w, \;\; f'(0) = 1, \;\; \theta(0) = 1, \;\; \phi(0) = 1, \\ f'(\infty) &= \varepsilon, \;\; \theta(\infty) = 0, \;\; \phi(\infty) = 0, \end{aligned} \tag{4.10}$$

$$M = \frac{\sigma B_0^2}{\rho a}, \; \varepsilon = \frac{b}{a}, \; \Pr = \frac{\mu c_p}{\kappa}, \; Sc = \frac{\nu}{D}, \; \gamma = \frac{R}{a}, \; f_w = \frac{-v_w}{\sqrt{a\nu}}, \tag{4.11}$$

where M (magnetic variable), ε (velocity ratio variable), $\Pr$ (Prandtl number), Sc (Schmidt number), γ (chemical variable) and f_w is blowing/suction variable with, $f_w < 0$ signifying blowing, $f_w > 0$ demonstrating suction and $f_w = 0$ equivalent to an impermeable sheet.

Expression for C_{fx}, Nu_x and Sh_x are

$$C_{fx} = \frac{-\mu}{\rho U_w^2}\left(\frac{\partial u}{\partial y}\right)_{y=0}, \; Nu_x = \frac{-x}{(T_w - T_\infty)}\left(\frac{\partial T}{\partial y}\right)_{y=0}, \; Sh_x = \frac{-x}{(C_w - C_\infty)}\left(\frac{\partial C}{\partial y}\right)_{y=0}, \tag{4.12}$$

obtaining the final dimensionless form by applying Eq. (4.6) in Eq. (4.12)

$$\left(\frac{\mathrm{Re}_x}{2}\right)^{1/2} C_{fx} = -f''(0), \; \left(\frac{2}{\mathrm{Re}_x}\right)^{1/2} Nu_x = -\theta'(0), \; \left(\frac{2}{\mathrm{Re}_x}\right)^{1/2} Sh_x = -\phi'(0), \tag{4.13}$$

where $\mathrm{Re}_x = \sqrt{\frac{a}{\nu}}x$ (the local Reynold number).

4.2 Homotopic procedure

The best choice of initial solutions and linear operators are

$$f_0(\eta) = \left(1 - \exp(-\eta)\right)(1 - \varepsilon) + \varepsilon\eta + f_w +, \; \theta_0(\eta) = \exp(-\eta), \; \phi_0(\eta) = \exp(-\eta), \tag{4.14}$$

$$\mathbf{L}_f[f] = f''' - f', \; \mathbf{L}_\theta[\theta] = \theta'' - \theta, \; \mathbf{L}_\phi[\phi] = \phi" - \phi, \tag{4.15}$$

with

$$\mathbf{L}_f\left[\tau_1^* + \tau_2^* \exp(\eta) + \tau_3^* \exp(-\eta)\right] = 0, \tag{4.16}$$

$$\mathbf{L}_{\theta}\left[\tau_4^{*}\exp(\eta)+\tau_5^{*}\exp(-\eta)\right]=0, \tag{4.17}$$

$$\mathbf{L}_{\phi}\left[\tau_6^{*}\exp(\eta)+\tau_7^{*}\exp(-\eta)\right]=0, \tag{4.18}$$

in which τ_i^{*} $(i=1-7)$ are unknown coefficients (constants).

4.2.1 Deformation statements of zeroth-order

$$(p-1)\mathbf{L}_f\left[f(\eta;p)-f_0(\eta)\right]=-pH_f\hbar_f\mathbf{N}_f\left[f(\eta;p)\right], \tag{4.19}$$

$$(p-1)\mathbf{L}_{\theta}\left[\hat{\theta}(\eta;p)-\theta_0(\eta)\right]=-pH_{\theta}\hbar_{\theta}\mathbf{N}_{\theta}\left[\hat{\theta}(\eta;p),f(\eta;p)\right], \tag{4.20}$$

$$(p-1)\mathbf{L}_{\varphi}\left[\hat{\phi}(\eta;p)-\phi_0(\eta)\right]=-pH_{\phi}\hbar_{\phi}\mathbf{N}_{\phi}\left[\hat{\phi}(\eta;p),f(\eta;p)\right], \tag{4.21}$$

$$f(0;p)=f_w,\quad f'(0;p)=1 \text{ and } f'(\eta;p)\to\varepsilon \text{ as } \eta\to\infty, \tag{4.22}$$

$$\hat{\theta}(0;p)=1 \text{ and } \hat{\theta}(\eta;p)\to 0 \text{ as } \eta\to\infty, \tag{4.23}$$

$$\hat{\phi}(0;p)=1 \text{ and } \hat{\phi}(\eta;p)\to 0 \text{ as } \eta\to\infty, \tag{4.24}$$

$$\mathbf{N}_f\left[f(\eta,p)\right]=f'''-f'^{2}+ff''+\varepsilon^2+M^2\left(\varepsilon-f'\right), \tag{4.25}$$

$$\mathbf{N}_{\theta}\left[\hat{\theta}\ (\eta;p), f\ (\eta;p)\right]=\hat{\theta}^{''}+\Pr f\ \hat{\theta}^{'}, \tag{4.26}$$

$$\mathbf{N}_{\phi}\left[\hat{\phi}\ (\eta;p), f\ (\eta;p)\right]=\hat{\phi}^{''}+Sc f\ \hat{\phi}^{'}-Sc\gamma\hat{\phi}, \tag{4.27}$$

where $\left(\mathbf{N}_{f},\mathbf{N}_{\theta},\mathbf{N}_{\phi}\right)$ are corresponding non-linear operators, $\left(\hbar_{f},\hbar_{\theta},\hbar_{\phi}\right)$ are the auxiliary parameters whereas $p\in[0,1]$ is an embedding parameter.

For $p=0$ and $p=1$, we have the following initial and final solution:

$$f\ (\eta;0)=f_{0}(\eta),\ \ f\ (\eta;1)=f\ (\eta), \tag{4.28}$$

$$\hat{\theta}(\eta;0)=\theta_{0}(\eta),\ \hat{\theta}(\eta;1)=\theta(\eta), \tag{4.29}$$

$$\hat{\phi}(\eta;0)=\phi_{0}(\eta),\ \hat{\phi}(\eta;1)=\phi(\eta), \tag{4.30}$$

4.2.3 Deformation systems of nth-order

$$\mathbf{L}_{f}\left[\ f_{n}(\eta)-\chi_{n}f_{n-1}(\eta)\ \right]=\hbar_{f}\mathbf{R}_{n}^{f}\ (\eta), \tag{4.31}$$

$$\mathbf{L}_{\theta}\left[\theta_{n}(\eta)-\chi_{n}\theta_{n-1}(\eta)\ \right]=\hbar_{\theta}\mathbf{R}_{n}^{\theta}\ (\eta), \tag{4.32}$$

$$\mathbf{L}_{\phi}\left[\phi_{n}(\eta)-\chi_{n}\phi_{n-1}(\eta)\ \right]=\hbar_{\phi}\mathbf{R}_{n}^{\phi}\ (\eta), \tag{4.33}$$

$$f_{n}^{'}(0)=0,\ f_{n}(0)=0\ \text{and}\ f_{n}^{'}(\infty)=0, \tag{4.34}$$

$$\theta_n(0) = 0 \text{ and } \theta_n(\infty) = 0, \tag{4.35}$$

$$\phi_n(0) = 0 \text{ and } \phi_n(\infty) = 0, \tag{4.36}$$

$$\mathbf{R}_n^f(\eta) = f_{n-1}'''(\eta) + (\varepsilon^2 + \varepsilon M)(1-\chi_{n-1}) - \sum_{k=0}^{n-1}\left[f_{n-1-k}' f_k' - f_{n-1-k} f_k'' \right] - M^2 f_{n-1}'(\eta), \tag{4.37}$$

$$\mathbf{R}_n^\theta(\eta) = \theta_{n-1}''(\eta) + \Pr \sum_{k=0}^{n-1}\left[\theta_k' f_{n-1-k} \right], \tag{4.38}$$

$$\mathbf{R}_n^\phi(\eta) = \phi_{n-1}''(\eta) - Sc\gamma\phi_{n-1}(\eta) + Sc\sum_{k=0}^{n-1}\left[f_k \phi_{n-1-k}' \right], \tag{4.39}$$

$$\chi_n = \begin{cases} 0, & \text{when } n \le 1, \\ 1, & \text{when } n > 1. \end{cases}, \tag{4.40}$$

where p variations between 0 to 1, $\left(f(\eta;p), \widehat{\theta}(\eta;p), \widehat{\phi}(\eta;p) \right)$ deform from the initial results $\left(f_0(\eta), \theta_0(\eta), \phi_0(\eta) \right)$ to the final results $\left(f(\eta), \theta(\eta), \phi(\eta) \right)$ correspondingly. By applying Taylor series, we have

$$f(\eta;p) = f_0(\eta) + \sum_{n=1}^{\infty} f_n(\eta)\, p^n \quad \text{with} \quad f_n(\eta) = \frac{1}{n!} \frac{\partial^n f(\eta;p)}{\partial p^n}\bigg|_{p=0}, \tag{4.41}$$

$$\widehat{\theta}(\eta;p) = \theta_0(\eta) + \sum_{n=1}^{\infty} \theta_n(\eta)\, p^n \quad \text{with} \quad \theta_n(\eta) = \frac{1}{n!} \frac{\partial^n \widehat{\theta}(\eta;p)}{\partial p^n}\bigg|_{p=0}, \tag{4.42}$$

$$\widehat{\phi}(\eta;p)=\phi_0(\eta)+\sum_{n=1}^{\infty}\phi(\eta)\,p^n \quad \text{with} \quad \phi_n(\eta)=\frac{1}{n!}\frac{\partial^n\widehat{\phi}(\eta;p)}{\partial p^n}\bigg|_{p=0}. \tag{4.43}$$

By choosing the suitable values of $(\hbar_f,\hbar_\theta,\hbar_\phi)$ and $p=1$. We have the convergent series solutions

$$f(\eta)=f_0(\eta)+\sum_{n=1}^{\infty}f_n(\eta), \tag{4.44}$$

$$\theta(\eta)=\theta_0(\eta)+\sum_{n=1}^{\infty}\theta_n(\eta), \tag{4.45}$$

$$\phi(\eta)=\phi_0(\eta)+\sum_{n=1}^{\infty}\phi_n(\eta). \tag{4.46}$$

The general solutions in terms of special solutions f_n^*, θ_n^* and ϕ_n^* are

$$f_n(\eta)=f_n^*(\eta)+\tau_1^*+\tau_2^*\exp(\eta)+\tau_3^*\exp(-\eta), \tag{4.47}$$

$$\theta_n(\eta)=\theta_n^*(\eta)+\tau_4^*\exp(\eta)+\tau_5^*\exp(-\eta), \tag{4.48}$$

$$\phi_n(\eta)=\phi_n^*(\eta)+\tau_6^*\exp(\eta)+\tau_7^*\exp(-\eta). \tag{4.49}$$

4.3 Convergence of the homotopic solutions

Eqs. (4.44-4.46) give us an analytical result of the system in series method. The convergence of the constructed series solutions can be attained by adjusting the auxiliary variables $\hbar_f$, $\hbar_\theta$ and $\hbar_\phi$. The $(\hbar_f,\ \hbar_\theta,\ \hbar_\phi)$-curves are sketched in Figs. (4.2-4.4) to adjust the convergence of the gained

series results. It is detected that the permitted ranges of $\hbar_f$, $\hbar_\theta$ and $\hbar_\phi$ are $-1.85 \le \hbar_f \le -0.5$, $-1.4 \le \hbar_\theta \le -0.5$ and $-1.95 \le \hbar_\phi \le -0.5$. The range of suitable values of $\left(\hbar_f, \hbar_\theta, \hbar_\phi\right)$ is clearly represented by the line parallel to η-axis. Table 4.1 is made to get the series solutions convergence. This table makes it clear that the homotopic solutions for velocity components converge at 10^{th} order of approximations whereas temperature and concentration are converges at 15^{th} order of approximations.

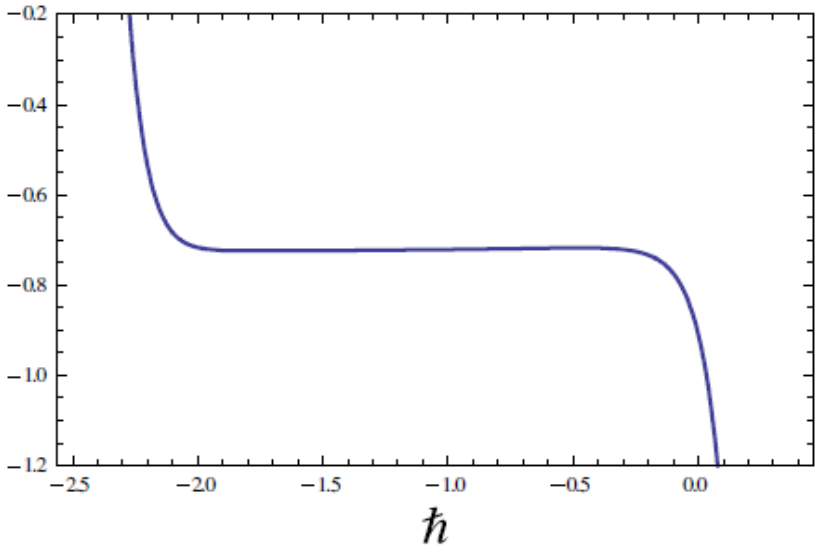

Fig. 4.2: $\hbar$-curve for $f(\eta)$.

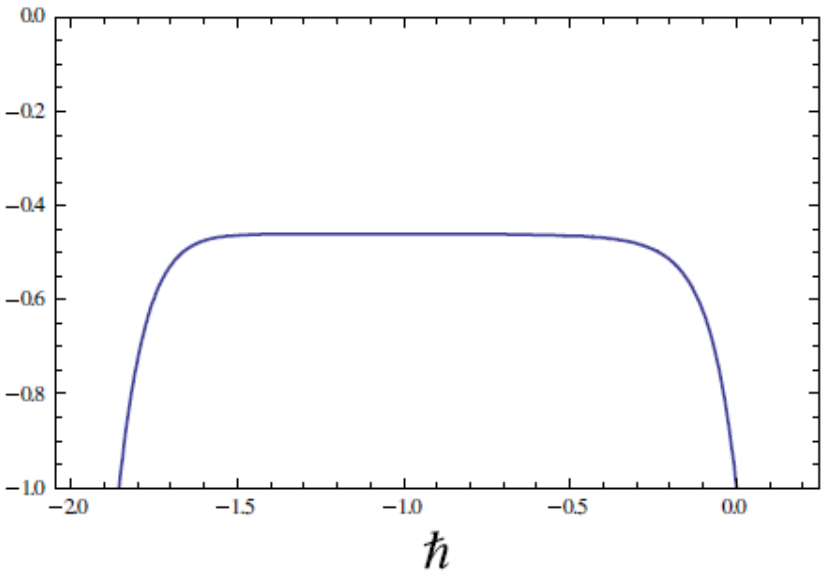

Fig. 4.3: $\hbar$ -curve for $\theta(\eta)$.

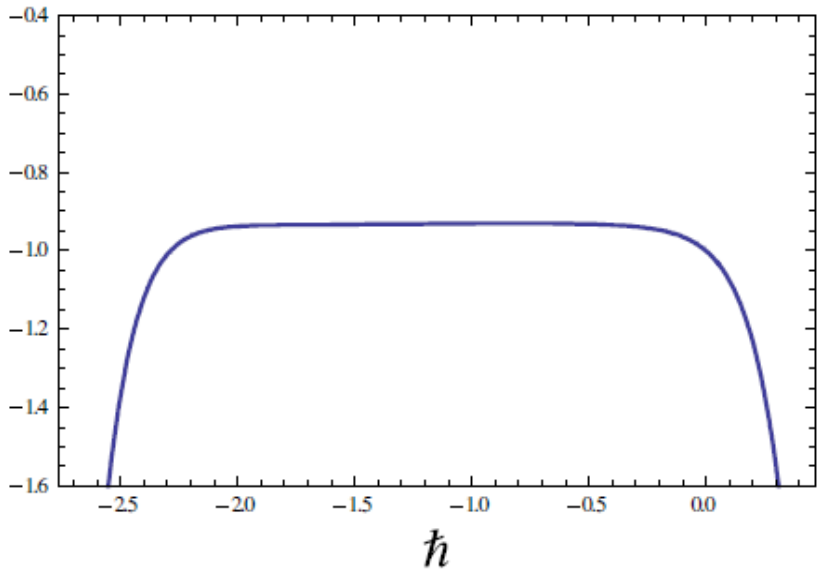

Fig. 4.3: $\hbar$ -curve for $\phi(\eta)$.

Table 4.1: Homotopic solution convergence for $M = \varepsilon = 0.1,\ \Pr = Sc = 1.0$ and $\gamma = 0.5$.

Order of approximation	$-f''(0)$	$-\theta'(0)$	$-\phi'(0)$
1	1.20374	1.24749	0.97749
5	1.26368	1.27698	0.99873
10	1.26377	1.29911	1.01518
15	1.26377	1.30187	1.01519

20	1.26377	1.30187	1.01519
25	1.26377	1.30187	1.01519
30	1.26377	1.30187	1.01519

Graphical discussion

5.1 Velocity fields

Present setion 5 focuses the impact of sundry variables on the $f'(\eta)$, $\theta(\eta)$, $\phi(\eta)$, C_{fx}, Nu_x and Sh_x profiles. Fig. 5.5 indicates that $f'(\eta)$ is reduces with higher values of M. Physically an enhancement in M results in a rise of Lorentz field force, which is opposed to the transport process, demonstrating that the transverse magnetic field opposes the transport characteristics. An enhancement in M causes the electric and magnetic fields in the electrically conducting liquid to interact, increasing the Lorentz field force. More resistance to the phenomena of transport is produced by this larger Lorentz force. The hydrodynamic boundary layer thickness reduction is more pronounced the greater the value of M. Moreover, Fig. 5.5 shows that $f'(\eta)$ rises with an increase in ε. Features of f_w versus $f'(\eta)$ is encountered in Figs. 5.6. It can be seen that the velocity layer thickness is diminished with the higher value of f_w.

5.2 Temperature fields

The impact of M on $\theta(\eta)$ is reported in Fig. 5.7. The features of M (Hartmann number) is to enhance $\theta(\eta)$ since M diminishes the flow field. Fig. 5.8 demonstrates the variation of ε versus $\theta(\eta)$. Here, we found that a rise in ε causes $\theta(\eta)$ inside the thermal boundary layer to drop, which in turn allows the thickness of the thermal boundary layer to diminish. Fig. 5.9 demonstrates the report of f_w on the $\theta(\eta)$ (dimensionless temperature). It is closely studied that when suction is

used instead of injection parameter f_w, the thermal boundary layer thickness decreases significantly.

5.3 Concentration fields

Fig. 5.10 is plotted for the dimensionless concentration field against Sc. It is observable that $\phi(\eta)$ and its corresponding boundary thickness layer reduce for higher values of Sc. Fig. 5.11 shows the variations of f_w versus $\phi(\eta)$. Concentration profile diminishes with the larger values of f_w. In Fig. 5.12 the properties of the γ (chemical reaction) on $\phi(\eta)$ are displayed. For larger γ, the $\phi(\eta)$ (concentration field) and its layer thickness diminishes. Influence of ε on $\phi(\eta)$ is presented in Fig. 5.13. Here $\phi(\eta)$ increases with the higher of ε.

5.4 Skin friction coefficient and local Nusselt and Sherwood numbers

Fig. 5.14 reported that growing M enhances the skin friction coefficient at the wall for all values of f_w (injection/suction variable). Physically in view of the magnetic field which diminishes the thickness of momentum layer and dimensionless velocity, and thus upsurges the velocity gradient. Coefficient of skin friction decreases with ε is also captured in Fig. 5.14. The characteristics of local Nusselt number versus $\Pr$, f_w and ε are revealed in Fig. 5.15. The local Nusselt number enhances with an increase in f_w (suction/injection variable). With suction, the local Nusselt number at the sheet/surface is found to be higher and diminishes without suction. It is also witnessed that local Nusselt number upsurges with $\Pr$ and ε. Fig. 5.16 depicts the behavior of local Sherwood number with M and Sc in the occurrence/absence of γ (chemical species parameter). Here we witnessed that mass transfer rate (local Sherwood number) is opposite response for higher values of Sc and M.

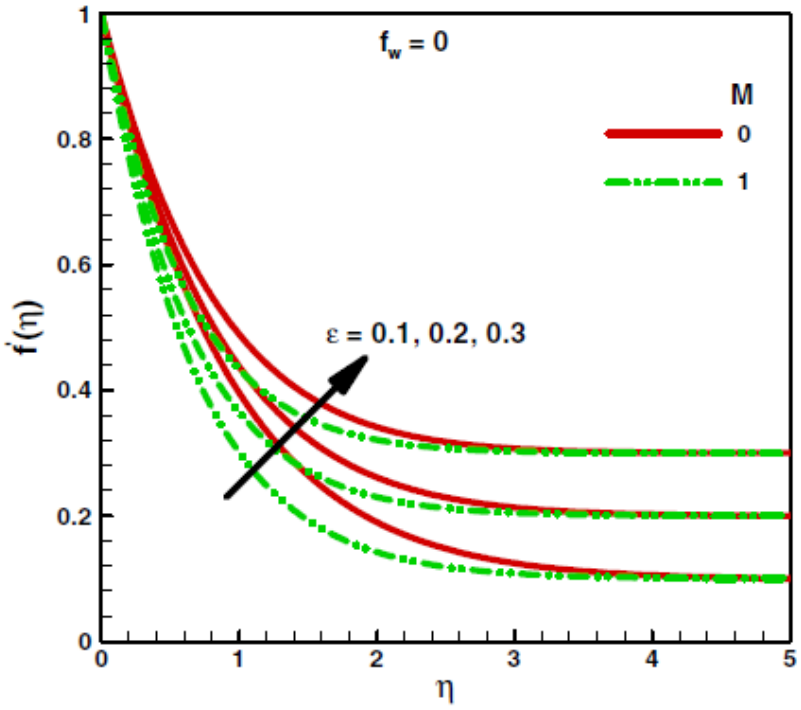

Fig. 5.1: ε and M features on $f'(\eta)$.

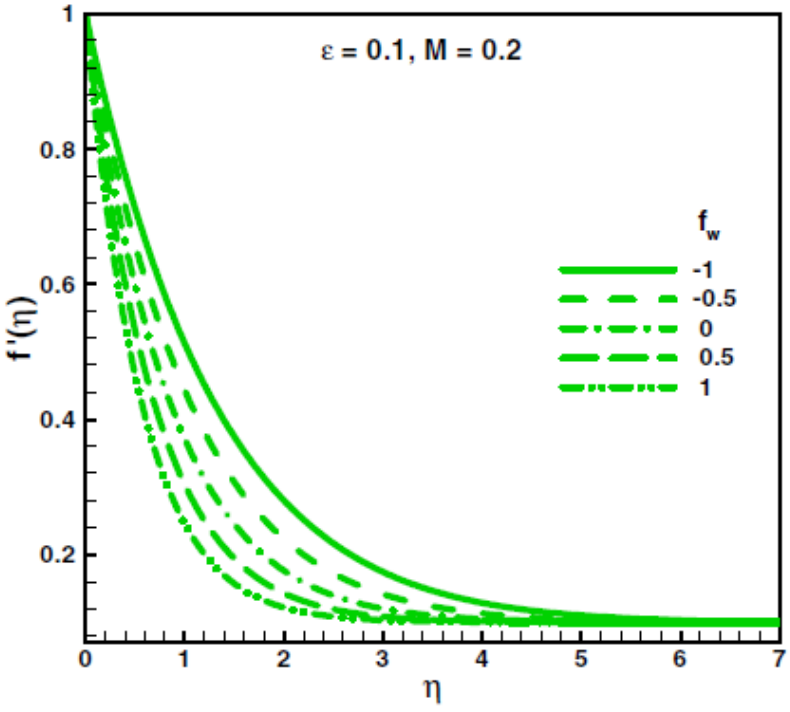

Fig. 5.2: f_w features on $f'(\eta)$.

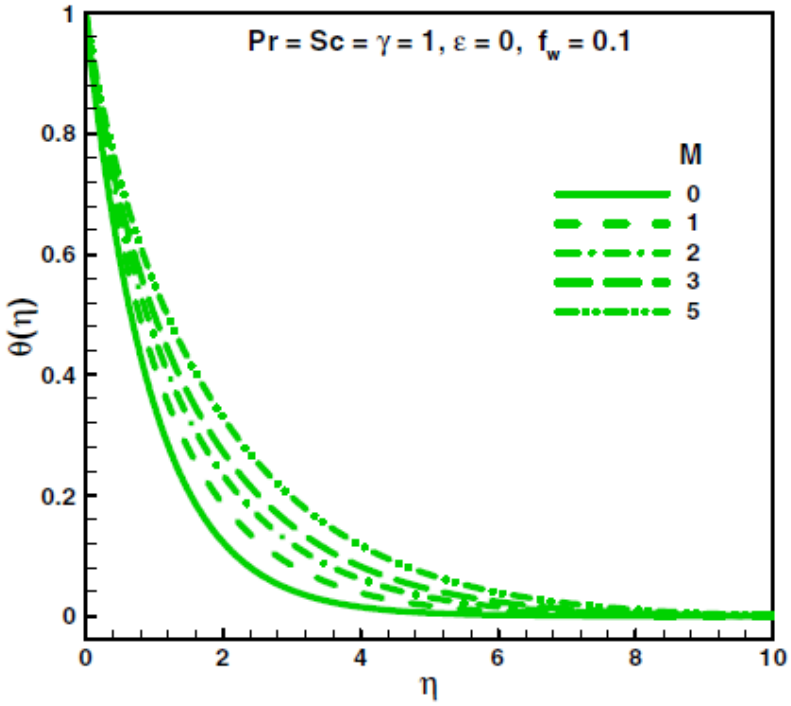

Fig. 5.3: M features on $\theta(\eta)$.

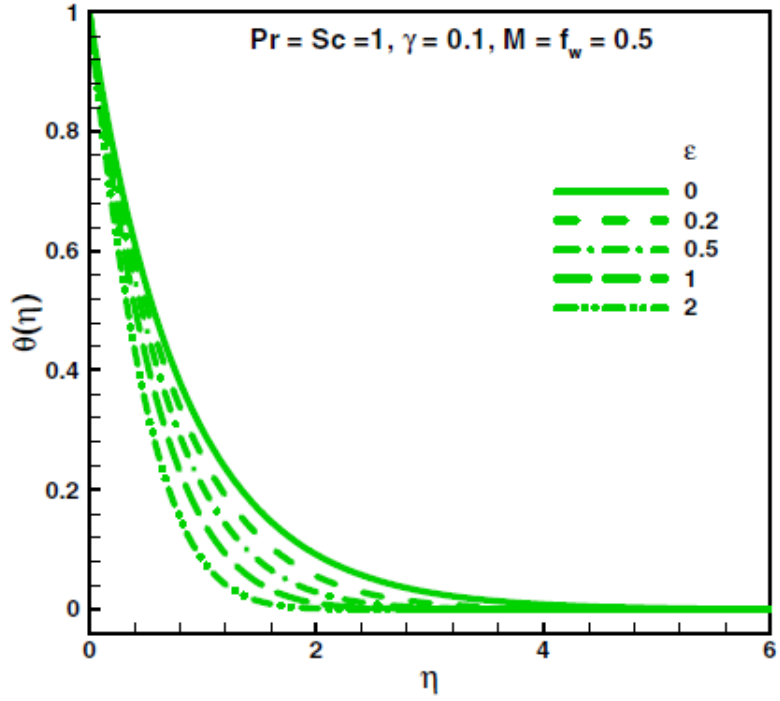

Fig. 5.4: ε features on $\theta(\eta)$.

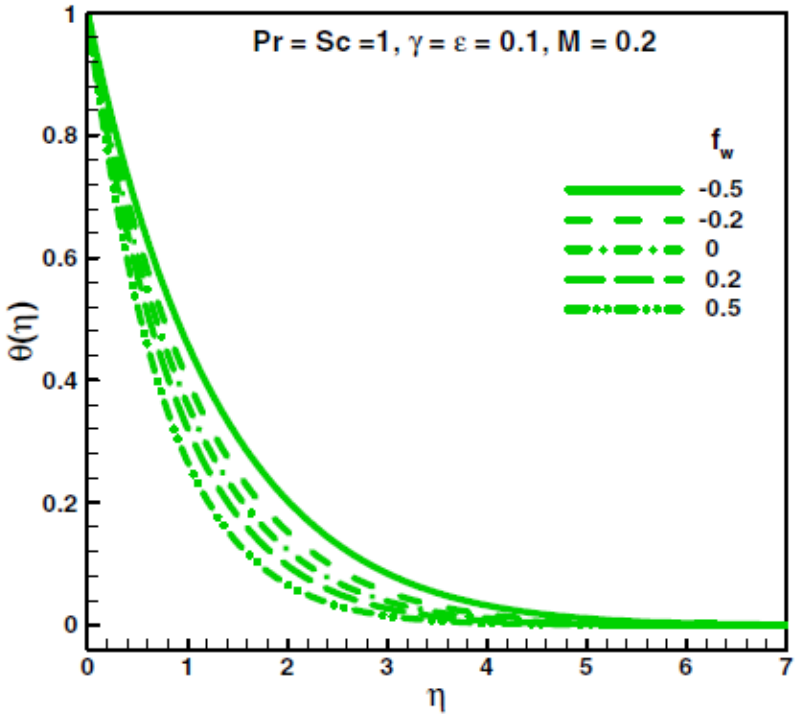

Fig. 5.5: f_w features on $\theta(\eta)$.

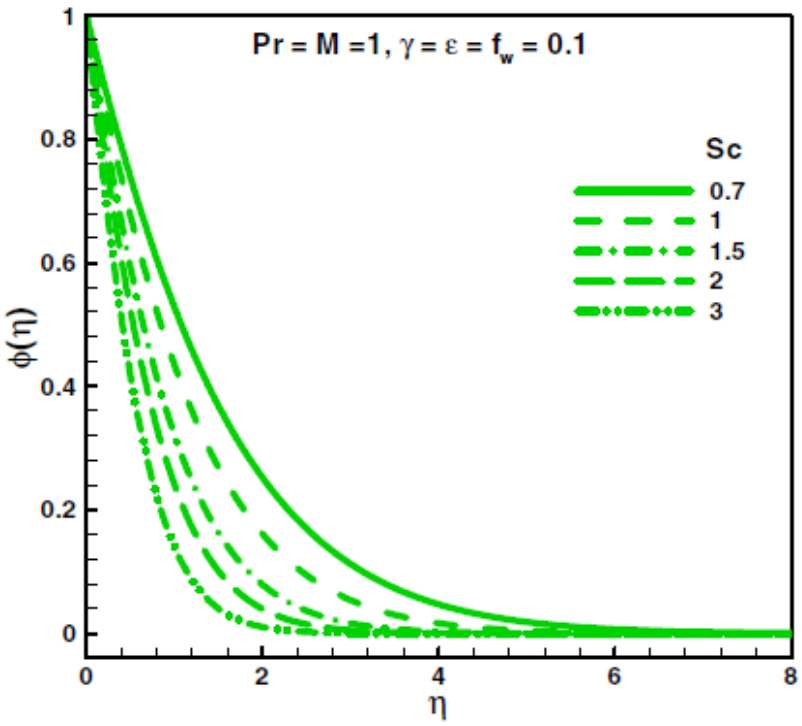

Fig. 5.6: Sc features on $\phi(\eta)$.

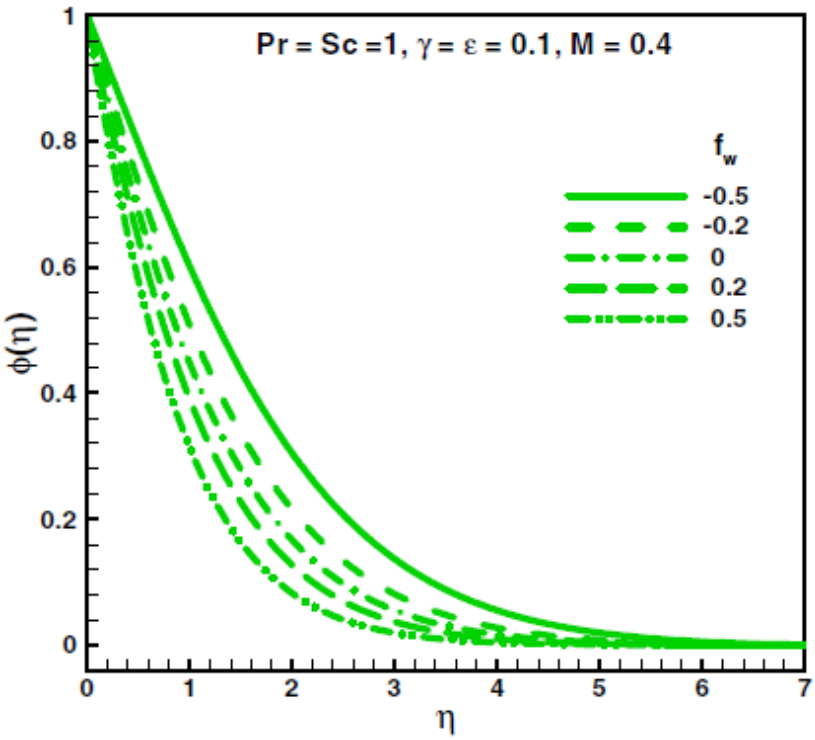

Fig. 5.7: f_w features on $\phi(\eta)$.

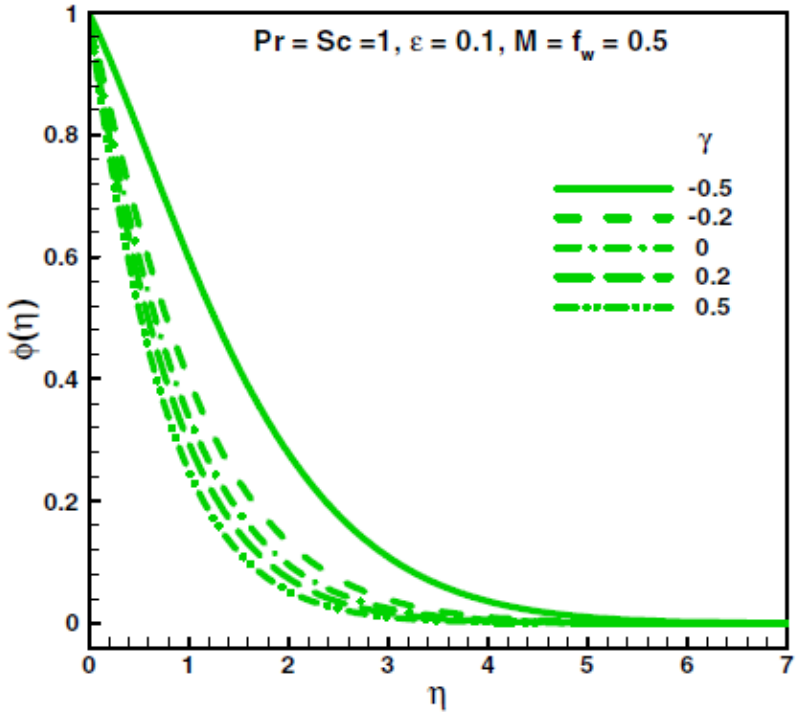

Fig. 5.8: γ features on $\phi(\eta)$.

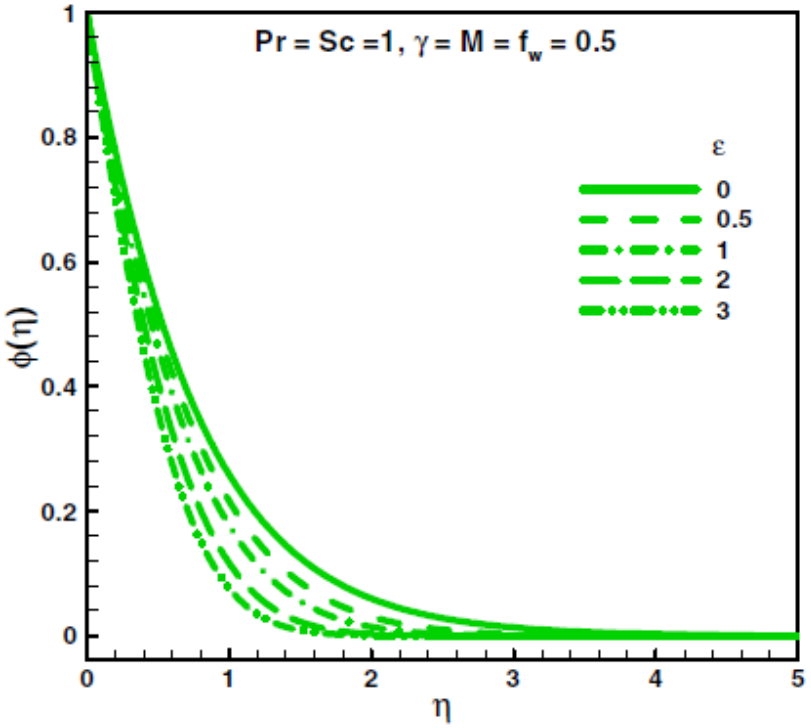

Fig. 5.9: ε features on $\phi(\eta)$.

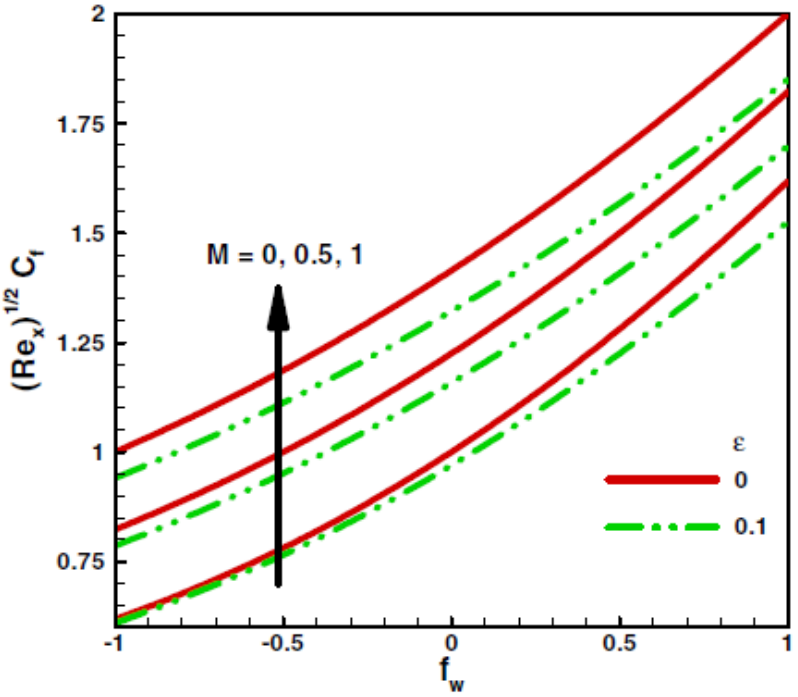

Fig. 5.10: f_w, M and ε features on $\mathrm{Re}_x^{1/2} C_{f_x}$.

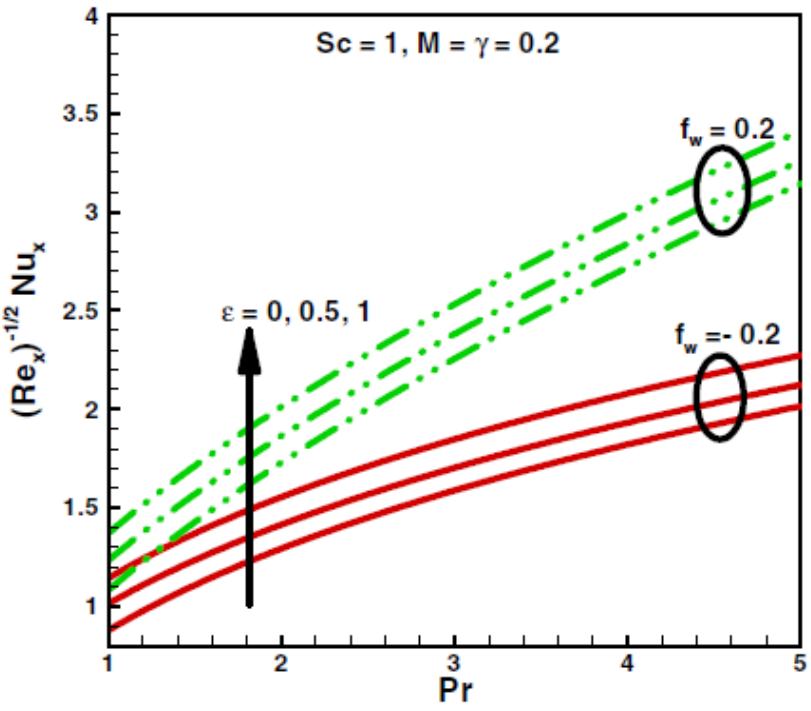

Fig. 5.11: Pr, f_w and ε features on $\mathrm{Re}_x^{-1/2} Nu_x$.

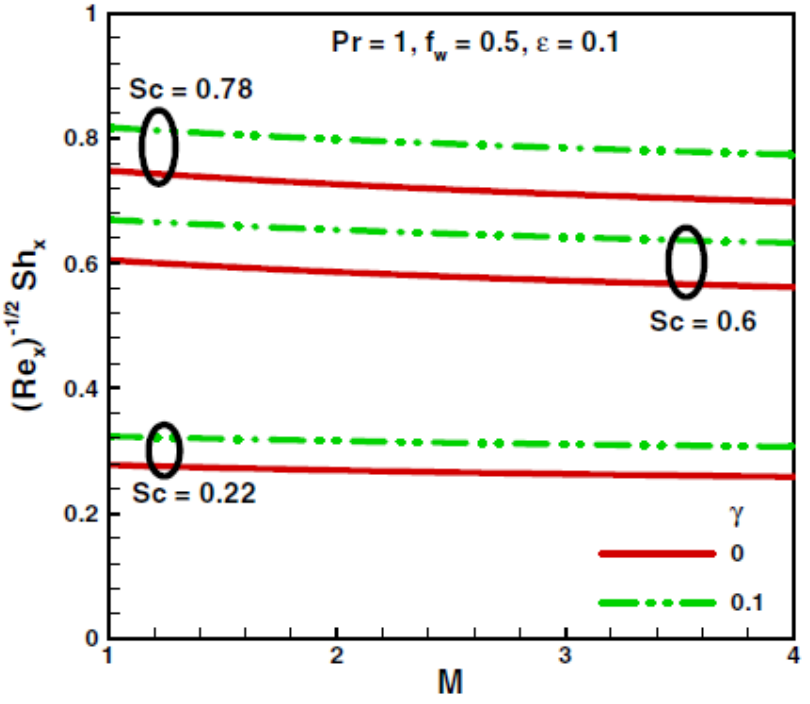

Fig. 5.12: M, ε and Sc features on $\mathrm{Re}_x^{-1/2} Sh_x$.

5.5 Closing remarks

This Section studies MHD stagnation point steady flow with heat and mass transport along a stretching permeable wall containing chemical reaction employing the homotopy analysis approach (HAM). The important conclusions of this analysis are summed up as below:

- Similar behavior of velocity field in frame of M and f_w.
- $\theta(\eta)$ and its thickness layer are decreasing function of ε.
- For larger values of Sc and γ, $\phi(\eta)$ (concentration sketch) and its thickness layer retards.
- Opposite features of skin friction coefficient and Sherwood number in view of M.
- Heat transfer rate (Nusselt number) is increased by enhancing Pr and ε.

Conclusion and future research work

This section 6 consists of conclusion and future research work.

6.1 Conclusion

MHD heat and mass transfer flow of viscous fluid through a permeable stretching sheet are delineated with stagnation point and chemical reaction. All the results are obtained in view of homotopic approach (HAM).

- Nonlinear ODEs are obtained through similarity transformation.
- Velocity field is decreasing aspects for larger values of f_w.
- $\theta(\eta)$ and its thickness layer are decreasing function of Pr.
- For larger γ, $\phi(\eta)$ (concentration sketch) and its thickness layer retards.
- Opposite features of skin friction coefficient and Sherwood number in view of M.
- Heat transfer rate (Nusselt number) is increased by enhancing Pr and ε.
- Mass transfer rate is opposite response for higher values of Sc and M.

6.2 Future research work

Literature survey reveals that most of the work in the past is concerned with the flows of Newtonian and non-Newtonian traditional heat transfer fluids. Proper attention is not given to the suspended nano-sized particles into the base fluid. In future I will concentrate on these fluid models with various techniques.

• References

[1] Crane, L. J. (1970). Flow past a stretching plate, Z. Anegew. Math. phys., 21, 645-647.

[2] Vajravelu, K. and Cannon, J. R. (2006). Fluid flow over a nonlinearly stretching sheet, Appl. Math. Comput., 181, 609-618.

[3] Ariel, P. D. (2003). Generalized three-dimensional flow due to a stretching sheet, J. Appl. Math. Mech., 83, 844-852.

[4] Andersson, H. I. Hansen, O. R. and Holmedal, B. (1994). Diffusion of a chemically reactive species from a stretching sheet, Int. J. Heat Mass Transf., 37, 659-664.

[5] Ali, F. M. Nazar, R. Arifin, N. M. and Pop, I. (2011). MHD boundary layer flow and heat transfer over a stretching sheet with induced magnetic field, Springer link, 47, 155-162.

[6] Khan, M. S. Alam, M. M. and Ferdows, M. (2013). Effects of Magnetic Field on Radiative Flow of a Nanofluid Past a Stretching Sheet, Procedia Eng., 56, 316-322.

[7] Abo-Eldahab, E. M. Adel, R. Mobarak, H. M. and Abdelhakem, M. (2021). The effects of magnetic field on boundary layer nano-fluid flow over stretching Sheet, Appl. Math. Inf. Sci. An Int. J., 6, 731-741.

[8] Turkyilmazoglu, M. (2017). Mixed convection flow of magnetohydrodynamic micropolar fluid due to a porous heated/cooled deformable plate: Exact solutions, Int. J. Heat Mass Transf., 106, 127-134.

[9] Chen, L. Zheng, X. and Ni, M. (2023). Numerical study of MHD mixed convection flow in the EU DEMO WCLL breeding blanket, Fusion Eng. Design, 194, 113906.

[10] Lu, H. B. Mazet, N. and Spinner, B. (1996). Modelling of gas-solid reaction Coupling of heat and mass transfer with chemical reaction, Chem. Eng. Sci., 51, 3829-3845.

[11] Arshad, M. Hussain, A. Hassan, A. Shah, S. A. G. A. Elkotab, M. A. Gouadria, S. Alsehli, M. and Galal, A. M. (2022). Heat and mass transfer analysis above an unsteady infinite porous surface with chemical reaction, Case Stud. Therm. Eng., 36, 102140.

[12] Qayyum, S. Hayat, T. and Alsaedi, A. (2017). Chemical reaction and heat generation/absorption aspects in MHD nonlinear convective flow of third grade nanofluid over a nonlinear stretching sheet with variable thickness, Results Phys., 7, 2752-2761.

[13] Hayat, T. Qayyum, S. Shehzad, S. A. and Alsaedi, A. (2017). Chemical reaction and heat generation/absorption aspects in flow of Walters-B nanofluid with Cattaneo-Christov double-diffusion, Results Phys., 7, 4145-4152.

[14] Qayyum, S. Hayat, T. Shehzad, S. A. and Alsaedi, A. (2017). Effect of a chemical reaction on magnetohydrodynamic (MHD) stagnation point flow of Walters-B nanofluid with newtonian heat and mass conditions, Nuclear Eng. Tech., 49, 1636-1644.

[15] Bai, Y. Wang, X. and Zhang, Y. (2023). Unsteady oblique stagnation point flow with improved pressure field and fractional Cattaneo-Christov model by finite difference-spectral method, Computers & Mathematics with Applications, 147, 38-52.

[16] Chu, Y. M. Al-Buriahi, M. S. Khan, A. A. Katub, K. M. S. Saqlain, M. Abbas, S. Z. and Khan**,** W. A. (2023). Significance of generalized Fourier and Fick's law and stagnation point flow for magnetized viscoelastic liquids, Mater. Sci. Eng. B, 296, 116602.

[17] Gupta, P. S. and Gupta, A. S. (1977). Heat and mass transfer on a stretching sheet with suction or blowing, Can. J. Chem. Eng., 55, 74-746.

[18] Hsiao, K. L. (2016). Stagnation electrical MHD nanofluid mixed convection with slip boundary on a stretching sheet, Appl. Therm. Eng., 98, 850-861.

[19] Bhattacharyya, K. (2011). Effects of radiation and heat source/sink on unsteady MHD boundary layer flow and heat transfer over a shrinking sheet with suction/injection. Front. Chem. Sci. Eng., 5, 376-384.

[20] Abel, M. S., Khan, S. K. and Prasad, K. V. (2001). Convective heat and mass transfer in a viscoelastic fluid flow through a porous medium over a stretching sheet, Int. J. Numer. Methods Heat Fluid Flow, 11, 779-792.

[21] Hayat, T. Shafiq, A. Alsaedi, A. and Awais, M. (2013). MHD axisymmetric flow of a third grade fluid between stretching sheets with heat transfer, Comput. Fluids, 86, 103-108.

[22] Rashidi, M. M. Mehr, N. and Rostami, B. (2012). Analysis of Entropy generation of MHD fluid flow due to a stretching rotating disk, Int. Confer. Mater. Eng. Adv. Tech., 10-12.

[23] Bhattacharyya, K. Mukhopadhyay, S. and Layek, G. C. (2012). Reactive solute transfer in magnetohydrodynamic boundary layer stagnation point flow over a stretching sheet with suction/blowing., Chem. Eng. Comm., 199 368-383.

[24] Ramesh, G. K. Gireesha, B. J. and Bagewadt, C. S. (2012). MHD flows of a permeable stretching sheet with non-uniform source/sink, Int. J. Heat Mass Transf., 55, 4900-4907.

[25] Das, K. (2011). Effect of chemical reaction and thermal radiation on heat and mass transfer flow of MHD micropolar fluid in a rotating frame of reference, Int. J. Heat Mass Transf., 54, 3505-3513.

[26] Chakraborty, B. K. and Mazumdar, H. P. (2000). MHD flow of Newtonian fluid over a stretching sheet, Approx. Theory Appl., 16, 32-41.

[27] Qayyum, S. Hayat, T. Alsaedi, A. and Ahmad, B. (2017). Magnetohydrodynamic (MHD) nonlinear convective flow of Jeffrey nanofluid over a nonlinear stretching surface with variable thickness and chemical reaction, Int. J. Mech. Sci., 134, 306-314.

[28] Dash, G. C. Tripathy, R. S. Rashidi, M. M. and Mishra, S. R. (2016). Numerical approach to boundary layer stagnation-point flow past a stretching/shrinking sheet, J. Mol. Liq., 221, 860-866.

[29] Jalilpour, B. Jafarmadar, S. Rashidi, M. M. Ganji, D. D. Rahime, R. and Shotorban, A. B. (2018). MHD non-orthogonal stagnation point flow of a nanofluid towards a stretching surface in the presence of thermal radiation, Ain Shams Eng. J., 9, 1671-1681.

[30] Rashidi, M. M. Ganesh, N. V. Hakeem, A. K. A. and Ganga, B. (2014). Buoyancy effect on MHD flow of nanofluid over a stretching sheet in the presence of thermal radiation, J. Mol. Liq., 198, 234-238.

[31] Sheikholeslami, M. Ganji, D. D. Javed, M. Y. and Ellahi, R. (2015). Effect of thermal radiation on magnetohydrodynamics nanofluid flow and heat transfer by means of two phase model, J. Mag. Magnet. Mater., 374, 36-43.

[32] Pop, S. R. Grosan, T. and Pop, T. (2004). Radiation effect on the flow near the stagnation point of a stretching sheet, Tech. Mechanik, 25, 100-106.

[33] Elbashbeshy, E. M. Emam, T. G. El-Azab, M. S. and Abdelgaber, K. M. (2012). Effect of magnetic field on flow and heat transfer over a stretching horizontal cylinder in the presence of heat source/sink with suction/injection, J. Appl. Mech. Eng. 1, 1000106.

[34] Sharma, P. R. and Singh, G. (2009). Effects of variable thermal conductivity and heat source/sink on MHD flow near a stagnation point on a linearly stretching sheet, J. Appl. Fluid Mech., 2, 13-21.

[35] Xu, H. Pop, I. and You, X. C. (2013). Flow and heat transfer in a nano-liquid film over an unsteady stretching surface, Int. J. Heat and Mass Transf., 60, 646-652.

[36] Sheikholeslami, M. Ganji, D. D. Javed M. Y. and Ellahi, R. (2015). Effect of thermal radiation on magnetohydrodynamics nanofluid flow and heat transfer by means of two phase model, J. Mag. Magnet. Mater., 374, 36-43.

[37] Mahabaleshwar, U. S. Maranna, T. Perez, L. M. and Nayakar, S. N. R. (2023). An effect of Magnetohydrodynamic and radiation on axisymmetric flow of non-Newtonian fluid past a porous shrinking/stretching surface, J. Magn. Magnet. Mater., 571, 170538.

[38] Dey, S. and Mukhopadhyay, S. (2022). MHD nanofluid flow over an absorbent plate in company of chemical response and zero nanoparticle flux, Forces in Mech., 7, 100102.

[39] Qayyum, S. Hayat, T. Shehzad, S. A. and Alsaedi, A. (2017). Nonlinear convective flow of Powell-Erying magneto nanofluid with Newtonian heating, Results in Phys., 7, 2933-2940.

[40] Nadeem, S. Haq, R. U. and Akbar, N. S. (2013). MHD three-dimensional boundary layer flow of Caisson nanofluid past a linearly stretching sheet with convective boundary condition, IEEE Transf. Nanotech., 13, 109-115.

[41] Turkyilmazoglu, M. (2017). Mixed convection flow of magnetohydrodynamic micropolar fluid due to a porous heated/cooled deformable plate: Exact solutions, Int. J. Heat Mass Transf., 106 127-134.

[42] Sheikholeslami, M. Ganji, D. D. and Rashidi, M. M. (2016). Magnetic field effect on unsteady nanofluid flow and heat transfer using Buongiorno model, J. Magnet. Magnet. Mat., 416, 164-174.

[43] K. Vajravelu, Viscous flow over a nonlinearly stretching sheet, J. Appl. Math. Comput., 124 (2001) 281-288

[44] P. S. Gupta and A. S. Gupta, Heat and mass transfer on a stretching sheet with suction or blowing, J. Canad. Chem. Eng., 55 (1977) 744-746.

[45] Turkyilmazoglu, M. and Pop, I. (2013). Heat and mass transfer of unsteady natural convection flow of some nanofluids past a vertical infinite flat plate with radiation effect, Int. J. Heat Mass Transf., 59, 167-171.

[46] Rajput, S. Bhattacharyya, K. Pandey, A. K. and Chamkha, A. J. (2022). Unsteady axisymmetric flow of nanofluid on nonlinearly expanding surface with variable fluid properties, JCIS Open, 8, 100064.

[47] Mabood, F. Khan, W. A. Ismail, A. I. M. (2015). MHD stagnation point flow and heat transfer impinging on stretching sheet with chemical reaction and transpiration, Chem. Eng. J. 273, 430-437.

[48] Liao, S. (2004). On the homotopy analysis method for nonlinear problems. Appl. Math. Comput., 147, 499-513.